Matter

CellPress

Article

On-Mask Chemical Modulation of Respiratory Droplets

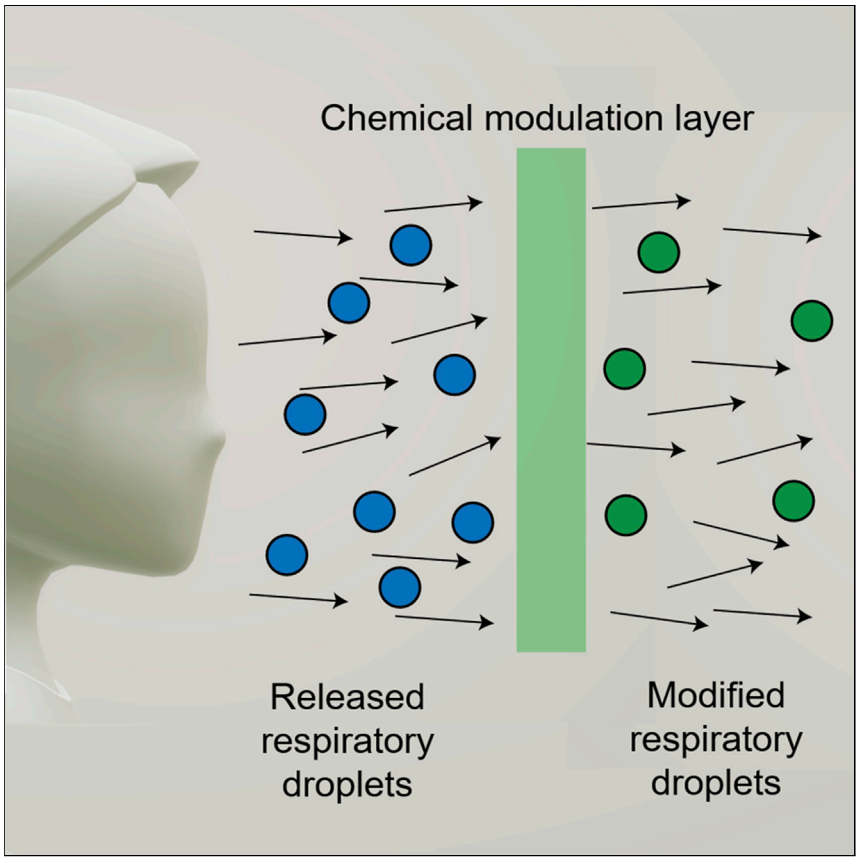

On-mask chemical modulation of model respiratory droplets is demonstrated, whereby a nonwoven mask layer is preloaded with antipathogen agents with the purpose of chemically contaminating escaped droplets to make them less infectious. Materials selection focuses on releasing these agents into the droplets in simulated sneezing and coughing, but not during simulated inhalation. It is found that even a low-fiber-density fabric can modify a significant fraction of escaped droplets.

Haiyue Huang, Hun Park, Yihan Liu, Jiaxing Huang

jiaxing-huang@northwestern.edu

HIGHLIGHTS

Polyaniline-coated, nonwoven fabrics serve as a reservoir to load antipathogen agents

Antipathogen agents are dissolved in escaped droplets and eventually concentrated

The degree of modification of the droplets is evaluated by microscopy imaging methods

Low-fiber-density fabrics can readily modify a significant fraction of escaped droplets

4 **Demonstrate**
Proof-of-concept of performance with intended application/response

Huang et al., Matter 3, 1791–1810
November 4, 2020
https://doi.org/10.1016/j.matt.2020.10.012

Matter

CellPress

Article

On-Mask Chemical Modulation of Respiratory Droplets

Haiyue Huang,[1,2] Hun Park,[1,2] Yihan Liu,[1] and Jiaxing Huang[1,3,*]

SUMMARY

Transmission of infectious respiratory diseases starts from pathogen-laden respiratory droplets released during coughing, sneezing, or speaking. Here we report an on-mask chemical modulation strategy, whereby droplets escaping a masking layer are chemically contaminated with antipathogen molecules (e.g., mineral acids or copper salts) preloaded on polyaniline-coated fabrics. A colorimetric method based on the color change of polyaniline and a fluorometric method utilizing fluorescence quenching microscopy are developed for visualizing the degree of modification of the escaped droplets by H^+ and Cu^{2+}, respectively. It is found that even fabrics with low fiber-packing densities (e.g., 19%) can readily modify 49% of the escaped droplets by number, which accounts for about 82% by volume. The chemical modulation strategy could offer additional public health benefits to the use of face covering to make the sources less infectious, helping to strengthen the response to the current pandemic or future outbreaks of infectious respiratory diseases.

INTRODUCTION

Viral respiratory diseases with epidemic potentials, such as influenza, SARS, MERS, and the current COVID-19 pandemic, represent a major global challenge that requires collaborative, holistic, and timely response.[1] For infection to occur, respiratory viruses must be transmitted from one person to another through the physical space. There should be many ways to set up physicochemical barriers to drastically reduce the number and viability of the viruses before they reach the host and breach the last line of biological and immunological defenses.[2] Public health measures to control and mitigate any infectious diseases must address one or more of the three necessary steps required for transmission (Figure 1). This includes identifying and isolating the source, breaking the chain of transmission, and protecting the susceptible hosts.[3–5] Transmission of infectious respiratory diseases starts from pathogen-laden respiratory fluid droplets released by an infected source during coughing, sneezing, singing, or even speaking, which can then propagate through several direct and indirect pathways to infect others.[6,7] Therefore, intervention methods that can reduce the amount (e.g., through the use of face covering) or the infectiousness of newly released droplets should be most useful, as they help to cut down the source and greatly reduce the burden of other control measures at later steps along the transmission pathways.[8]

Sneezing and coughing are violent expiratory activities accompanied by dynamic and complex liquid fragmentation, droplet ejection, and water evaporation, releasing a much higher flux of respiratory fluid compared with normal breathing. The ejected droplets are typically in the range of micrometers to millimeters in

Progress and Potential

Mask wearing has become a new norm in many parts of the world in the COVID-19 pandemic. There has been much interest in enhanced masks that can better protect the wearers. However, a mask or face covering is much more effective in protecting others because it can block and reroute a large portion of the virus-laden respiratory droplets from symptomatic or asymptomatic infected wearers. Here, we propose an on-mask chemical modulation strategy to enhance this function by making the escaped droplets less infectious. As a proof of concept, antipathogen agents (e.g., mineral acid and copper salt) preloaded on nonwoven fabrics are shown to transfer to and are concentrated in escaped droplets to the level capable of deactivating pathogens. We hope that this approach leads to additional work, which, if eventually adopted, can help to cut down the sources of transmission and strengthen the public health response to control and mitigate the outbreak of infectious respiratory diseases.

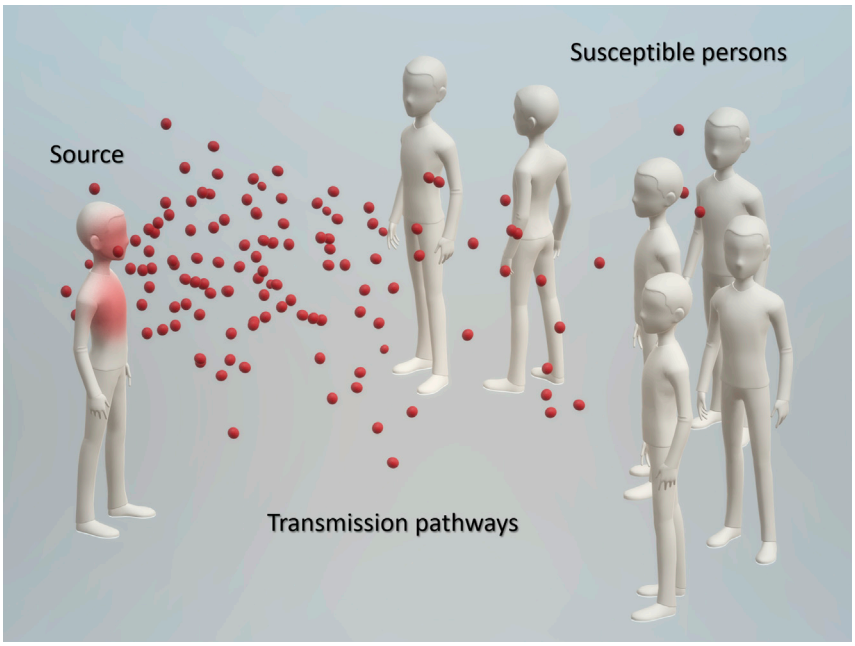

Figure 1. Three Necessary Steps for the Transmission of an Infectious Disease
A source that can release the pathogens, possible transmission pathways along which the pathogens remain structurally intact and infectious before eventually reaching other hosts, and susceptible persons that the pathogens can successfully infect to duplicate themselves and start a new cycle. Mitigation strategies must address one or more of these steps. Isolating the source or making it less infectious should be most effective, as it cuts down the source of the spread chain and greatly reduces the burden at the later stages along the transmission pathways.

size, and can travel at a speed of 10–20 m/s[7,9,10] Therefore, they can reach a distance of well over 4–6 m. Although the droplets are relatively large and can settle via gravity, after evaporation a certain fraction can turn into submicron-sized nuclei (i.e., dried or semidried mass of respiratory droplets) that can remain suspended in ambient air flow for an extended period of time.[11] The use of a face covering can drastically reduce the number of droplets and their forward traveling distance.[12–14] for this reason, in many parts of the world wearing a mask is strongly recommended and even mandated in public areas to prevent and slow down the spread of COVID-19.[15] There are a few types of masks commonly available: respirators (such as N95), surgical masks, and face coverings using common fabrics. Among these masks, respirators are designed to have the highest filtration efficiency and are best for protecting wearers in potentially high-viral-dosage environments, such as for healthcare workers. Surgical or so-called medical masks have a relatively lower filtration efficiency for ultrafine particles or droplets and are more effective in blocking outgoing droplets.[12] Recent reports showed that some common fabrics also have good performance[16,17] and may reduce the droplet transmission when widely implemented by the public, making them as possible substitutes when and where professional grades of masks are not widely available. In general, masks with higher fiber-packing density are more effective in blocking the droplets. However, they also make breathing more difficult. Moreover, more efficient droplet trapping can lead to accumulation of respiratory fluid in the masks, which not only decreases their efficacy but also turns them into a secondary source of virus-laden mist in exhalation cycles.[18]

Here, we report an alternative strategy that focuses on chemically altering respiratory droplets when they escape a masking layer to make them less infectious rather

[1]Department of Materials Science and Engineering, Northwestern University, Evanston, IL 60208, USA

[2]These authors contributed equally

[3]Lead Contact

*Correspondence:
jiaxing-huang@northwestern.edu

https://doi.org/10.1016/j.matt.2020.10.012

than blocking them completely. There has been increasingly high interest in chemically modified masks that can deactivate trapped pathogens on the outer surfaces, and these are usually designed to better protect wearers.[19–25] However, to the best of our knowledge, much less attention has been paid to improve or enhance face coverings for the purpose of better protecting others from the wearers, and chemical modulation of respiratory droplets has yet to be explored. A mask filters air both inward (i.e., during inhalation) and outward (i.e., during exhalation). Enhanced masks for better self-protection have been very appealing from the perspective of individual users. However, mask concepts for better protection of others from the wearer helps to address larger-scale public health needs to control and mitigate an outbreak of infectious respiratory diseases.

As shown in Figure 2A, a chemical modulation layer loaded with antipathogen agents can be inserted, such as an add-on or insert of common face-covering fabrics, to leach antipathogen agents into the outgoing droplets. Eventually, these solutes are drastically concentrated when droplets evaporate to yield dried or semidried respiratory nuclei, helping to deactivate pathogens. Proofs of concept are demonstrated using pneumatically generated droplets of model respiratory fluid to simulate coughing and sneezing. The droplets fly through a piece of low-density, nonwoven fabric (e.g., a medical gauze or lint-free wipe) coated with polyaniline doped with mineral acid or copper salt, and eventually land on a detector film for microscopy imaging. Colorimetric and fluorometric imaging methods are developed to visually differentiate modified and unmodified droplets received by the detector film. It is found that a single layer of gauze mask that barely hinders air-flow (i.e., with undetectable pressure drop) can readily modify about 19% of the penetrating droplets by number, which accounts for about 28% by volume. Using a lint-free wipe with low pressure drop comparable with that of a commercial protection mask, the number and volume fractions of modified droplets increase to about 49% and 82%, respectively. Importantly, air flows without the droplets, which reassemble the inhalation process, do not cause these agents to desorb. These results suggest that the chemical modulation of respiratory droplets, when used in conjunction with face covering, could bring significant additional benefits to mitigate the spread of infectious respiratory diseases, especially for those transmittable through presymptomatic or asymptomatic carriers such as COVID-19.

RESULTS AND DISCUSSION

Materials Selection

Release of antipathogen agents (e.g., chemicals or particles) should not be triggered during inhalation to avoid being transported to the respiratory tracts and lungs. Note that exhalation blows warm and wet air with droplets outward, while inhalation draws drier and colder air from the environment inward without droplets (Figure 2A). This excludes volatile or particulate modifiers that could desorb or detach from the fibers, which become a potential inhalation hazard. Therefore, nonvolatile molecular agents such as phosphoric acids and copper salts are selected because they can readily dissolve in droplets. A low pH environment (pH < 3) is generally suitable for disinfection because it denatures proteins and disrupts the lipid membrane in pathogens.[26,27] Ionic copper is a well-known broad-spectrum antimicrobial agent.[28,29] To enable loading of acid and copper ions on the nonwoven fabrics, the fibers are coated with a layer of conducting polymer polyaniline by *in situ* polymerization. Polyaniline is chosen for its ease of synthesis and its capability to noncovalently and reversibly bind mineral acids and metal cations.[30–33] Two types of

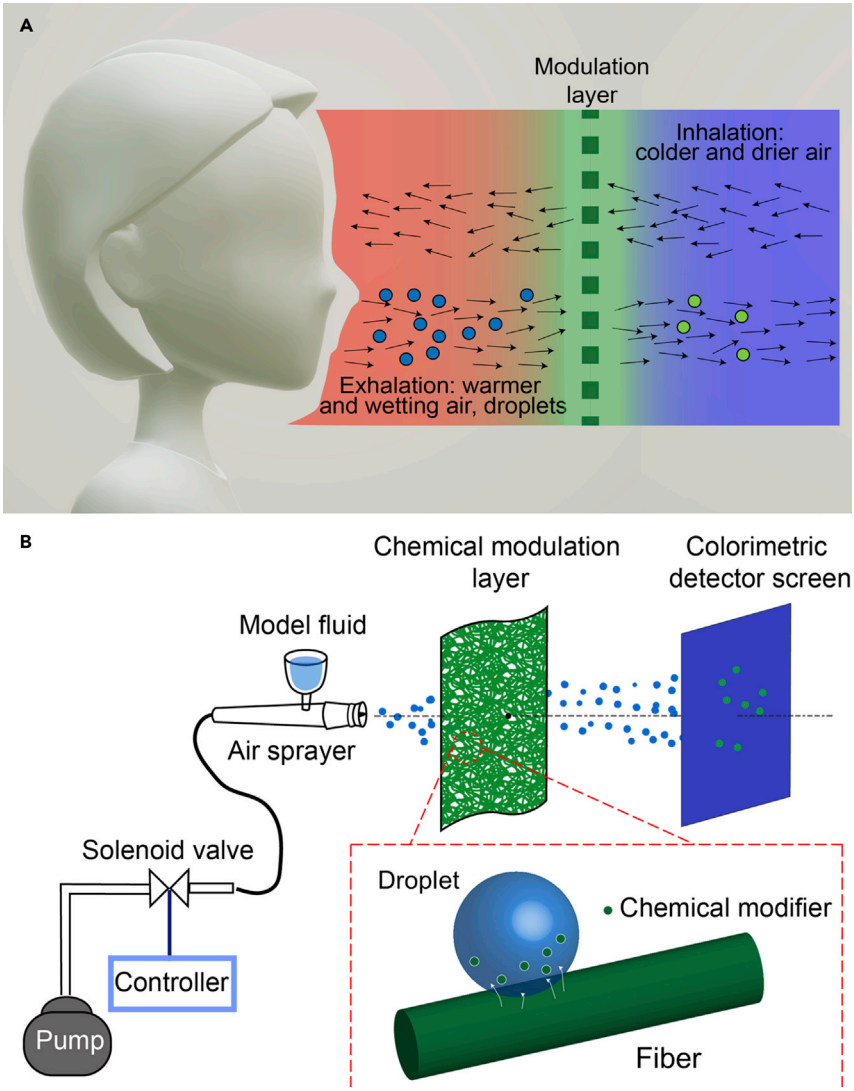

Figure 2. On-Mask Chemical Modulation of Respiratory Droplets: Hypothesis and Approach

(A) Exhalation pushes warmer and wetter air outward, along with respiratory droplets through the mask to the environment. In contrast, inhalation draws colder and drier air from the environment, but without droplets. A chemical modulation layer can be inserted to leach antipathogen agents into the outgoing droplets. To avoid inhaling antipathogen agents (e.g., chemicals or particles), their release mechanism should be activated by the droplets.

(B) In the experimental design, droplets of model respiratory fluids were pneumatically pulsed to simulate those released during coughing and sneezing with comparable range of size distribution, number density, and velocity. The droplets were directed toward a modulation layer (e.g., a nonwoven fabric loaded with chemical modifiers). A detector film was placed at the downstream to collect the escaped droplets, so that their degrees of chemical modification could be visualized directly.

nonwoven fabrics are tested as the model masking layer. One is a medical gauze cloth with around 11% of volumetric fiber density and nearly zero pressure drop. The other is a lint-free wipe commonly used for removing dust from surfaces in laboratories with around 19% of volumetric fiber density, which results in a pressure drop comparable with that of the commercial protection mask (Figure S1). These low-density fabrics do not hinder air flow and breathing significantly if used alone or with other types of face covering.

Experimental Setup to Simulate Coughing and Sneezing

As shown in Figure 2B, an air sprayer operated in a pulsed mode was used to simulate the process of coughing and sneezing. Studies related to respiratory droplets[34,35] often use a mixture of biopolymers, NaCl, and sometimes surfactants as artificial respiratory liquid. In this work, an aqueous solution of polyvinyl alcohol (PVA) and NaCl was poured into the sprayer as the model fluid. The solutes simulate the hygroscopic components in respiratory fluids and leave drying stains on the detector screen for location of the droplets and measurement of their sizes. The air-flow speed during pulsed spraying was set to 20 m/s, and the resulting droplets (collected 6 cm away from the nozzle) were found to be around 16–160 μm in diameter. The air-flow speed and the size distribution of the droplets are comparable with those generated by coughing and sneezing (Table S1). These droplets were blown toward a chemical modulation layer placed close to the nozzle. A colorimetric or fluorometric detector film was placed downstream to capture escaped droplets for analysis of their sizes and concentrations of chemical modifiers.

Preparation of the Chemical Modulation Layer

Polyaniline was coated on common fabrics as illustrated in Figure 3A. A roll of gauze or wipe was dipped into a monomer solution and then squeezed to remove the excess before being immersed in an oxidant solution to trigger the *in situ* polymerization, similar to the rapidly mixed reactions often used for synthesizing polyaniline dispersions.[31,36] The fibers serve as heterogeneous nucleation sites, facilitating the growth of polymer on their surface. After polymerization, the fabrics were rinsed with deionized water to remove by-products and weakly bonded polyaniline. To load phosphoric acid or copper sulfate, polyaniline-coated fabrics were soaked in the corresponding solutions for 30 min before rinsing with ethanol and air-drying.

Figures 3B and 3E are optical microscopy images of the pristine gauze and lint-free wipe taken under reflection mode, respectively, exhibiting nonwoven fiber mat structures. The difference in fiber-packing density is more distinguishable under transmission mode (Figure S2). Figures 3C and 3F are images of the gauze and wipe coated with acid-doped polyaniline, respectively. Both fabrics maintained their nonwoven structures after coating, indicating that the *in situ* polymerization process does not alter the microstructures of the fabrics. The color of the fabrics turned green, which is characteristic for the doped emeraldine salt form of polyaniline. Scanning electron microscopy (SEM) images of the coated gauze (Figure 3D) and wipe (Figure 3G) show that polyaniline indeed coated individual fibers rather than forming particles trapped in between the fibers.

Preparation of the Colorimetric Detector Film

Although the size distribution of fine droplets can be measured by microscopy and particle size analyzers,[37] simultaneous determination of the size and concentration of specific chemicals has been difficult. In this work, the concentration of phosphoric acids (i.e., pH) in the modified droplet was evaluated by a colorimetric detector film. Polyaniline was chosen again as the colorimetric indicator because it can be processed into insoluble films with high spatial uniformity and high color intensity. The color of polyaniline switches reversibly between green and blue upon doping by the acid and dedoping by the base, respectively. Therefore, droplets modified with a sufficiently high concentration of acid should induce a color change on the undoped detector film.

Figure 4A illustrates how the detector film was prepared. A white-colored smooth plastic film, such as the separator membrane used in batteries, was floated on the

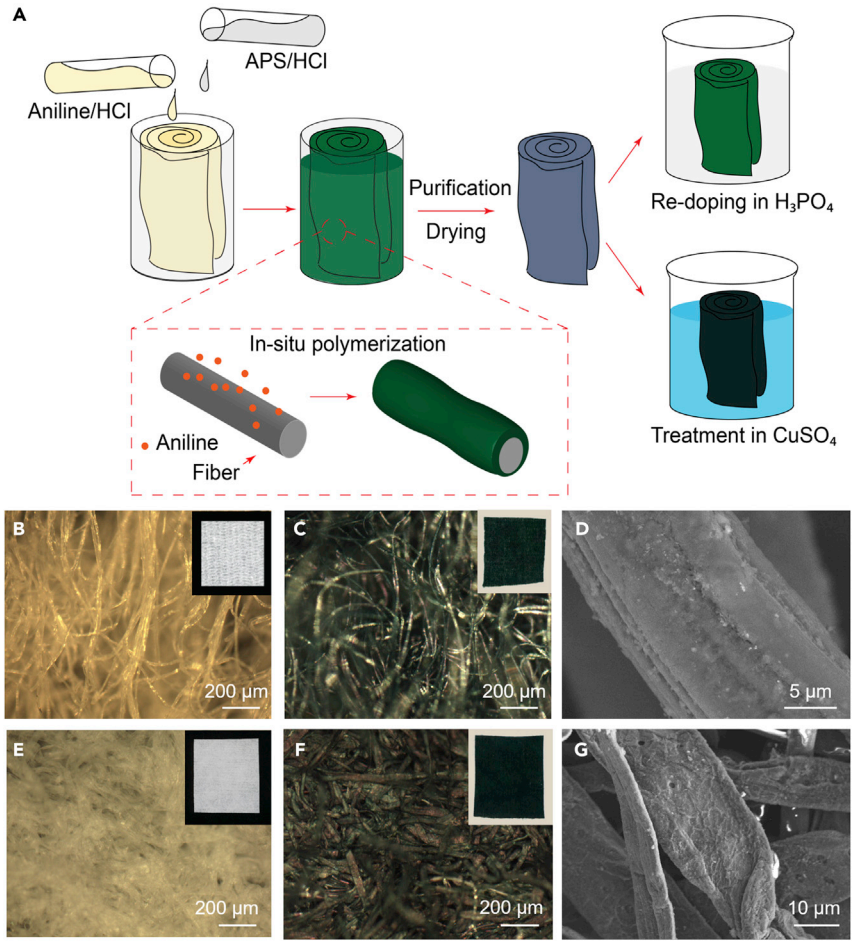

Figure 3. Preparation of the Chemical Modulation Layer

(A) A roll of nonwoven fabric was coated with polyaniline by *in situ* polymerization of aniline. The fabric was then washed with deionized water and dried in air. The polyaniline coating can be doped with molecular antipathogen agents such as mineral acids or Cu ions by soaking in H_3PO_4 or $CuSO_4$ solutions, respectively.

(B–G) Optical microscopy images showing the gauze fibers (B) before and (C) after polyaniline growth. The insets are photos of the gauze fabrics (2 cm × 2 cm). (D) SEM image of coated gauze fibers. Corresponding images of a lint-free wipe are shown in (E), (F), and (G).

surface of a polymerizing bath made of the monomer and the oxidant in HCl. After 10 min of reaction under magnetic stirring, a film of polyaniline was formed on the side in contact with the reactants (Figure 4B). The green film turned blue when rinsed with deionized water and dedoped in ammonium hydroxide (Figure 4C). The dedoped film exhibited high spatial uniformity even when observed under an optical microscope (Figure 4D), making it suitable for colorimetric differentiation of acid-modified and unmodified droplets. Figure 4E is an atomic force microscopy (AFM) image of the detector film, showing the edge of the film, where part of it was removed using Scotch tape. The film had a uniform thickness of about 100 nm throughout the scanned region (Figure 4F).

Colorimetric Visualization of Droplet Stains

The schematic drawings in Figures 5A and 5D explain how the degree of chemical modification of each droplet can be visualized. Since the model fluid contains PVA and NaCl, all the droplets landing on the detector film will leave topologically rough

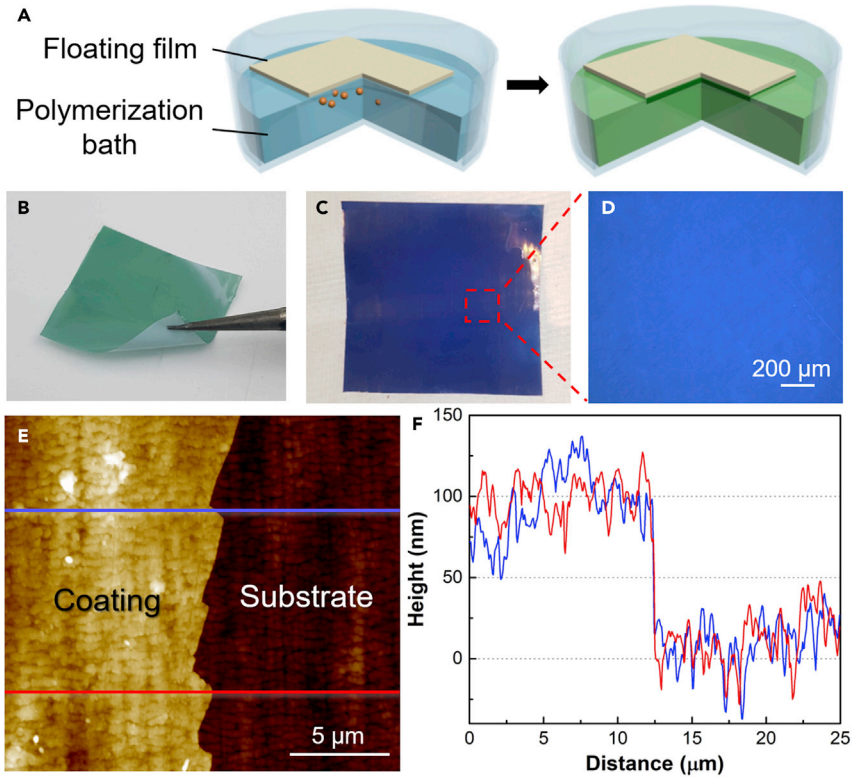

Figure 4. Preparation of the Colorimetric Detector Film

(A) A layer of polyaniline was grown on one side of a smooth plastic film floating on the surface of the polymerization bath.

(B–D) (B) The as-grown green film (5 cm × 5 cm) turned (C) blue after dedoping, which yielded (D) a highly uniform blue field of view under an optical microscope.

(E) AFM image showing a torn edge of the polyaniline layer.

(F) Height profiles taken from (E) show that the coating thickness is around 100 nm.

stains on the smooth detector film. Under the reflection mode of optical microscopy, these stains should appear as dark spots on a bright background due to a reduced level of reflection. Therefore, reflection mode can be used to locate all the droplets that landed on the detector film regardless of their pH values. The transmission mode is relatively insensitive to the roughness of the stains but can differentiate colors. Therefore, under transmission mode, stains of unmodified droplets should be barely visible (Figure 5A, right), but stains of modified droplets (Figure 5D, right) should appear as green dots on a blue background.

The colorimetric detector film was first tested with droplets sprayed through an uncoated gauze cloth. Indeed, dry stains of these unmodified droplets are highly visible under the reflection mode (Figure 5B). Since the undoped polyaniline is hydrophobic, it allows the landed droplets to bead up (see Figure S3 for contact angles), preventing them from spreading out. In conjunction with the viscosity of the fluid, this results in a well-defined contact line and eventually a clear edge of dried stain for each droplet, making it possible to calculate the size of droplets based on the size of their drying marks. Despite the large number of stains observed in the reflection mode, none of them can be clearly identified in the transmission mode (Figure 5C). In contrast, for droplets passing through a gauze (Figures 5E and 5F) or a wipe (Figures 5G and 5H) modified with H_3PO_4, many green dots are

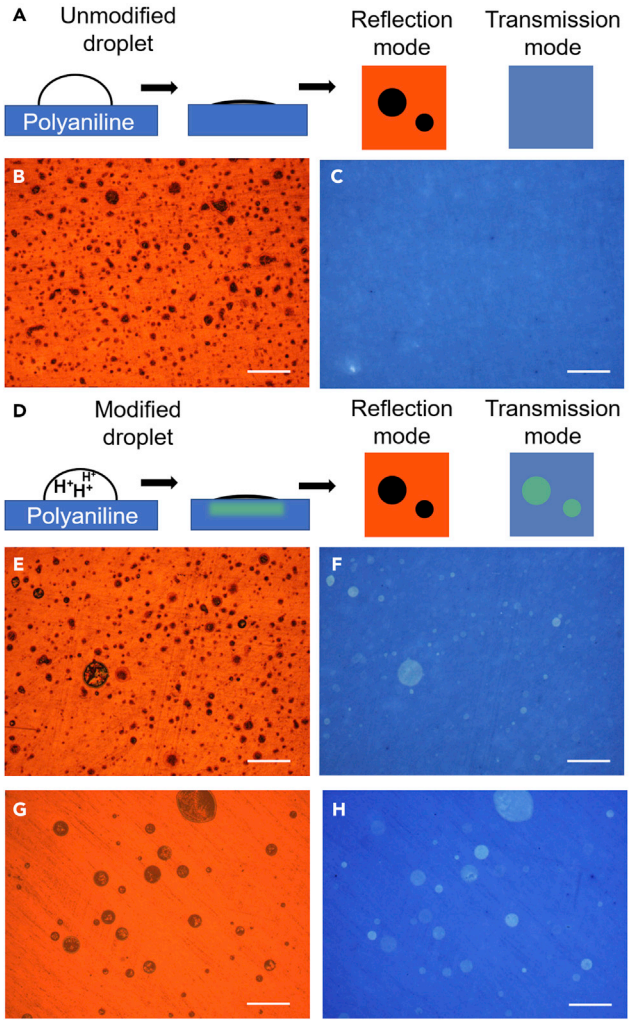

Figure 5. Colorimetric Visualization of Modified Droplets

(A–C) (A) Unmodified, nearly neutral droplets leave drying stains made of polymer and salts that are highly visible under (B) the reflection mode of imaging, but not under (C) the transmission mode. (D) In contrast, since modified droplets contain acid and can dope polyaniline, they leave green stains that are visible under both modes of imaging.

(E–H) (E and F) and (G and H) are representative images of stains of droplets passing through a gauze cloth and a lint-free wipe, respectively. Note that not all the droplets observed under the reflection mode (E and G) can be seen under the transmission mode, due to insufficient level of acid modification. All scale bars represent 200 μm.

clearly visible in the transmission images. By comparing the images taken under reflection mode (Figures 5E and 5G) and transmission mode (Figures 5F and 5H), droplets can be differentiated based on their degrees of acid modification, which can be used to determine the number and volumetric percentages of modified droplets.

Quantitative Analysis of Microscopy Images

The reflection and transmission images of the same area of view are used in conjunction to quantify the degree of acid modification for each droplet. Intuitively this includes two steps: locate all the droplets that land on the detector film based on the reflection image and then quantify the degree of modification based on the color

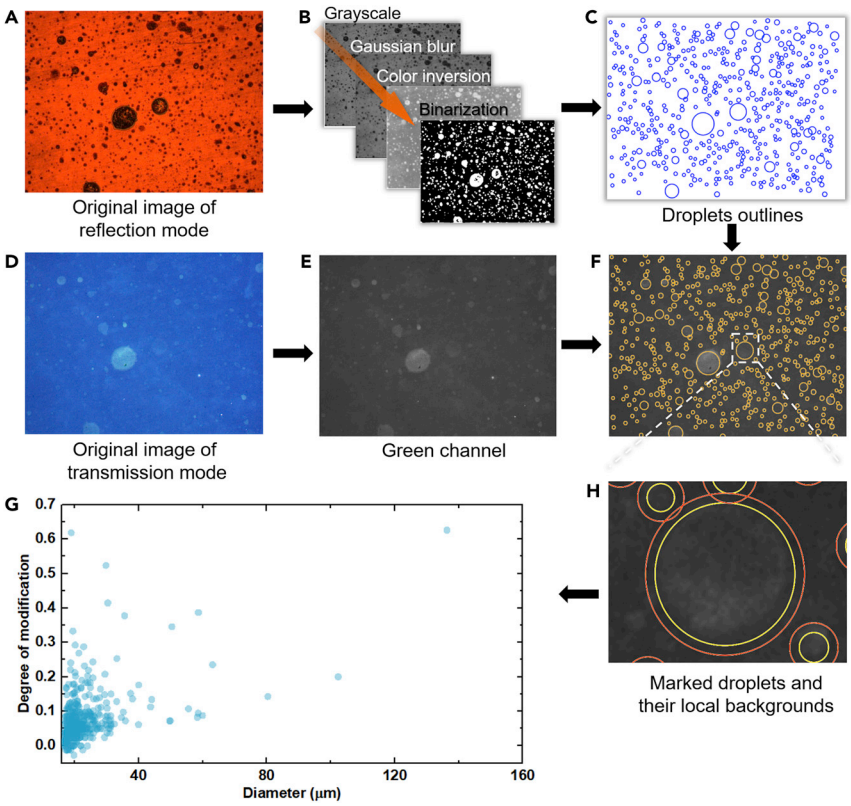

Figure 6. Quantitative Analysis of Colorimetric Microscopy Images

(A) Since both unmodified and modified droplets are visible in the reflection mode of image, it was used to create marks to identify the positions of all droplets in (D) the corresponding transmission mode of image, in which only modified droplets are visible.

(B) The reflection image underwent a few steps of processing to yield a noise-reduced, binarized image to prepare for recognition using Hough circle transformation.

(C) Eventually the droplets were approximated as circular marks, which were used to identify the locations and sizes of the droplets in the transmission image.

(D and E) (E) The green channel of (D) was extracted to calculate pixel intensity values.

(F–H) (F) By overlapping the marking patterns (C) and (E), the pixel intensity inside each droplet, as illustrated by the yellow circles in (H), can be measured, together with the pixel intensity of local background around each droplet (red circle). Pixel intensities inside and outside a droplet were used to calculate its degree of modification based on Equation 1 (see also Supplemental Information). Such analysis produced the calculated degree of modification of all droplets and their corresponding radii based on optical microscopy images from (A) and (D), which are plotted in (G). Each dot represents one droplet.

change in the transmission image. Overlaying the two images would have been a straightforward way to achieve this, but is distorted by some unwanted features such as rolling marks on the plastic film or accidental scratches. Therefore, the droplet marks in the reflection images are processed by the algorithm of Hough circle transformation[38] (Figure S4) and converted into a circular mask, which is then applied to the transmission images to locate the droplets. As illustrated in Figures 6A–6C, a color image under the reflection mode underwent several steps of preprocessing, including conversion to grayscale, Gaussian blur, color inversion, and binarization, before Hough circle transformation. The circular outlines were then overlapped on the green channel (Figures 6D and 6E) of the transmission image to evaluate the brightness (i.e., pixel intensity) inside each circle. The green channel was chosen because the modified droplets created green marks on the blue

background, which best represented the degree of acid doping of the polyaniline detector film. This created a composite image (Figure 6F) in which the size and pixel intensity of each circle were readily accessible.

In digital images, the brightness of each pixel corresponds to an intensity value between 0 and 255. The brightness of a droplet can then be calculated by averaging the pixel intensities of thousands of pixels. Therefore, the contrast in brightness, which is the greenness of the droplet stain, reflects the doping level of the underlying polyaniline spot and the degree of acid modification of the droplets by the chemical modulation layer. The contrast is defined as

$$\frac{I_d - I_b}{I_b} = \text{Degree of modification}, \qquad \text{(Equation 1)}$$

where I_d is the average value of all pixels within the top 50% of pixel intensity and I_b is the mode value of all pixels in the surrounding background (Figure 6H). The detailed processes are available in Supplemental Information and Figure S5.

Calibrating Degree of Modification Based on pH Values

Next, how the degree of modification is related to the pH value of the droplets was experimentally defined. In equilibrium, the onset of acid doping of polyaniline is normally around pH 4.[39] However, for volume-limited microscale droplets, lower pH values (i.e., higher concentrations of acid) are needed to dope a polyaniline film of finite thickness. As shown in Figure 7A, model fluids with pH values adjusted to 1.3, 1.6, 1.9, 2.1, 2.3, and 2.5 were sprayed onto the detector film to generate droplet marks with known pH values. As expected, the contrast of the droplet marks indeed decreased with increasing pH and eventually diminished at pH 2.5. The quantification process described in Figure 6 was then applied to analyze the microscopy images and yielded a distribution of degree of modification for droplets of each pH value (Figure 7B). The peak position of the control fluid with a pH around 6.0 (control) is around zero modification, and the degree of modification shifts to higher values with decreasing pH values. Model fluid with pH 2.5 can dope the polyaniline detector film at equilibrium, but the corresponding droplets did not produce sufficiently visible contrast, which is attributed to an insufficient amount of acid in the droplets and insufficient diffusion time before the droplets dried. Since the highest pH value of the droplets that can produce a detectable color change was 2.3, the threshold of acid modification was set at the peak of the pH 2.3 curve (Figure 7B, red dashed line), corresponding to a value of a degree of modification of 0.075. Therefore, only droplets with a degree of modification larger than 0.075 are counted as being modified hereafter. Since the pH value of the initial fluid is around 6.0, this threshold of modification represents an increase in acid concentration by at least 3.7 orders of magnitude for modified droplets. This is drawn rather conservatively to avoid over-representing the fraction of modified droplets.

Evaluation of Chemical Modification Efficiency by Nonwoven Fabrics

The droplet modification efficiency can be defined based on number (η_n) and volume (η_v) fractions:

$$\eta_n = \frac{\text{Number of modified droplets}}{\text{Number of all droplets collected}}, \qquad \text{(Equation 2)}$$

$$\eta_v = \frac{\text{Volume of modified droplets}}{\text{Volume of all droplets collected}}. \qquad \text{(Equation 3)}$$

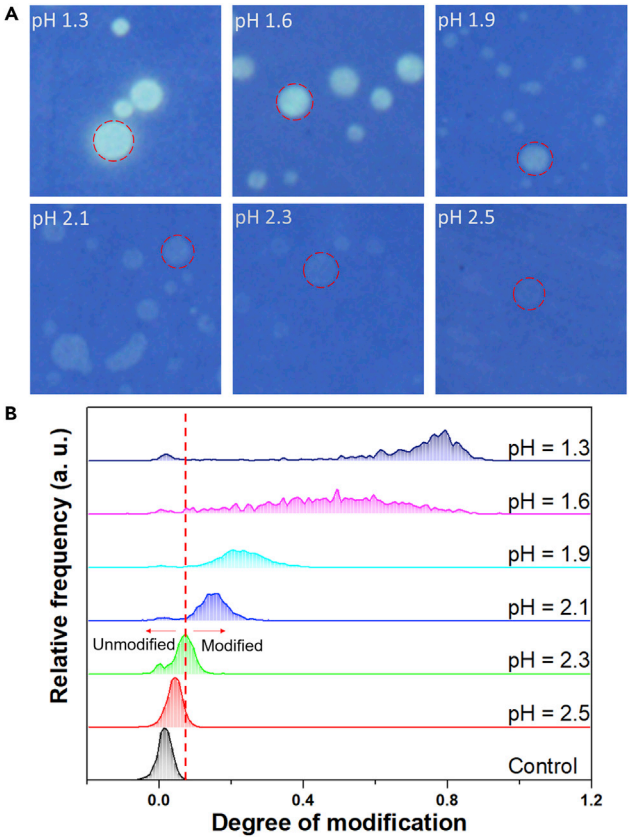

Figure 7. Calibration of the Degree of Modification

Droplets from stock solutions of six known pH values (1.3, 1.6, 1.9, 2.1, 2.3, and 2.5) were sprayed onto the colorimetric screen, and (A) the resulting images taken under transmission mode were used to calibrate (B) how the color changes (i.e., greener dot means higher degree of modification) correlate with the pH values of the droplets. Microscopy observation in (A) shows that for a droplet to produce a distinguishable green dot on the blue polyaniline film, its pH value needs to be $\leq$2.3. All images in (A) are 200 μm × 200 μm.

For η_n, the denominator is obtained by counting the number of all received droplets based on their dried marks on the colorimetric detector. The numerator is defined as the number of droplets with a degree of modification larger than 0.075. η_v can be regarded as η_n weighted by volume. Polyaniline-coated gauzes and wipes were tested, together with a control experiment in which the model fluid was sprayed through a piece of pristine gauze. The size and degree of modification for each collected droplet were measured and plotted in Figure 8. Each dot in Figures 8A–8C represents one droplet, and each plot includes results obtained from over 4,000 droplets (Table S2). For each plot, the distribution of droplet size and the degree of modification are also shown at the horizontal and vertical axes, respectively. The horizontal red dashed lines denote the modification threshold, and only droplets above this line were counted as modified. The volumetric densities of the gauze (Figure 8B) and lint-free wipe (Figure 8C) are only 11% and 19%, respectively, but both can modify significant fractions of droplets. η_n for the gauze and the wipe were calculated to be about 19% and 49%, respectively. The corresponding η_v values were 28% and 82%, respectively. Since the value of η_v is more sensitive to the large droplets, higher η_v values suggest that larger droplets are more likely to be modified by the fabrics. Figures 8B and 8C show that a higher number of large droplets (>50 μm in diameter) escaped from the wipe than from the gauze. This

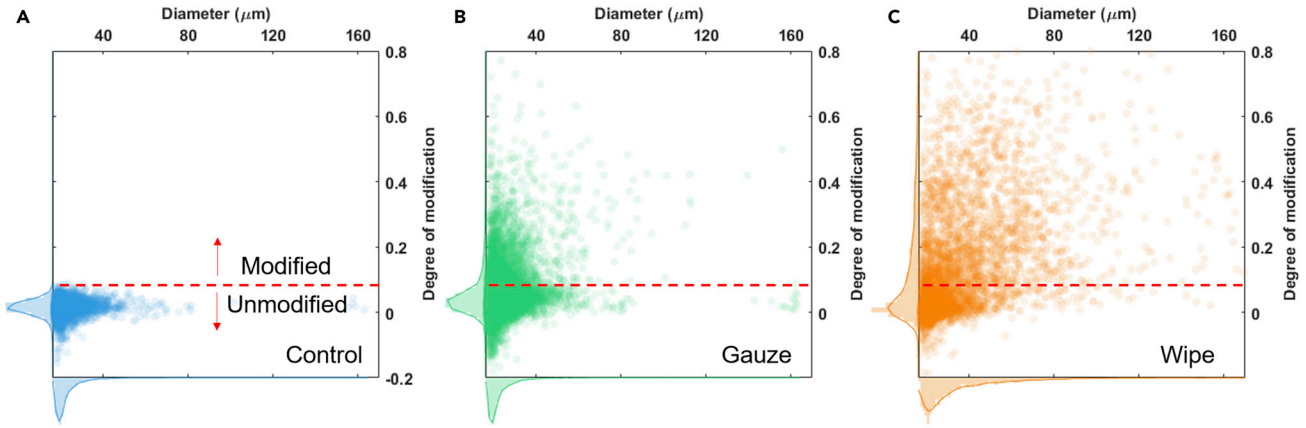

Figure 8. Effect of Droplet Modulation by the Gauze and Wipe

The histograms show the distributions of the size and the corresponding degree of modification of droplets, after they passed through (A) a blank gauze, (B) a gauze, and (C) a lint-free wipe coated with acid-doped polyaniline, respectively. Each dot represents one droplet on the detector screen, and each histogram consists of over 4,000 droplets. The red dashed lines denote the threshold of modification chosen to calculate modulation efficiency, which corresponds to the peak value of pH 2.3 curve in Figure 7B.

can be attributed to the coalescence of entrapped droplets within the fiber mat, which is more pronounced in higher-density fabrics. The above results show that a denser, thicker, or multilayer fabric with higher areal fiber density will increase the efficiency of droplet modification but will also lead to a larger pressure drop, making it more difficult to breathe. Therefore, to achieve optimized modifying efficiency, one would need to select a suitable range of fiber density based on the acceptable level of pressure drop during the entirety of application.

Droplet-Fiber Interactions

Droplets can escape from a nonwoven fiber network in three ways (Figure 9): (1) some small droplets can be carried through the network by air stream without colliding with any fiber; (2) some droplets collide with fibers without losing much kinetic energy and eventually bounce their way out of the network; (3) some droplets are caught by the fibers upon collision, and can then glide along the fibers and grow larger via coalescence with other droplets and/or condensation of water vapor.[40,41] Indeed, large droplets of around 100 μm in diameter trapped in between the fibers can often be observed under the optical microscope (Figure S6). Entrapped droplets can be released again, especially in higher-speed air flows (e.g., during coughing or sneezing) either as enlarged individual droplets or many smaller ones due to splitting, which is known as re-entrainment. Types 1–3 would lead to unmodified droplets, slightly modified droplets, and significantly modified droplets, respectively, based on the length of the retention time of droplet-fiber interactions. With thicker and denser layers of nonwoven fabrics, types 1 and 2 would diminish, but type 3 becomes the dominating factor. For virus-laden respiratory droplets, type-3 mechanism reduces the efficacy of face covering as it nebulizes entrapped fluid in the mask, regenerating fine mists of virus-containing droplets into the air.

The results obtained with fabrics with different fiber densities are consistent with the above analysis. The gauze layer allowed a larger number of droplets to pass through and resulted in a lower fraction of modified droplets. The wipe has nearly doubled fiber density and allowed much fewer and larger droplets to pass through, resulting in a much higher fraction of modified droplets. These observations suggest that droplets escaping from the lint-free wipe were dominated by the type-3 mechanism,

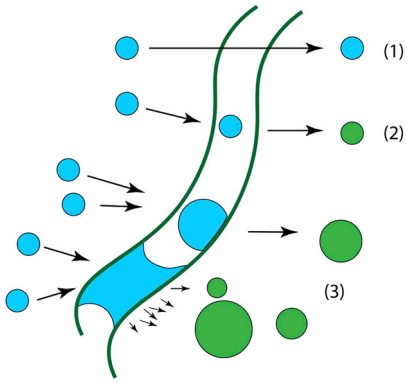

Figure 9. Possible Ways for Droplets to Escape the Modulation Layer

Schematic drawings showing that (1) droplets can escape the layer unmodified due to lack of any or significant interaction with the fibers, the fraction of which is largely determined by the packing density of the fabric; (2) droplets colliding with the fibers have higher chances of being modified; and (3) droplets can get caught on the fibers and grow larger through coalescence and/or condensation of water vapor, which leads to longer retention time (i.e., higher degree of modification), before they break apart via the air flow and escape.

which has the longest retention time of droplets for mass transfer and thus a higher degree of modification (Figure 8C).

The above analysis is intended to guide the materials selection of the fabric layer for the chemical modulation of droplets. Using a few layers of low-density fiber network or a single denser layer can drastically reduce type-1 and type-2 escaped droplets but increase type-3 droplets. This would lead to an entrapment problem for unmodified thick masks, but with the chemical modifier the entrapped fluids become less infectious either on the mask or after re-emission (type 3) by strong air flows during sneezing or coughing.

Droplets Modified by Copper-Loaded Fabrics

The methodology demonstrated for acid modification can be adopted to study the chemical modification of other agents. As a proof of concept, Figure 10 demonstrates chemical modulation of droplets by copper ions as well as fluorometric differentiation of droplets by their copper contents under a fluorescence microscope. Copper ion is a well-studied broad-spectrum antipathogen agent,[28,29] which can also be loaded on the polyaniline-coated fabrics to dissolve in the passing droplets.[32] The small volume of the collected droplets and the presence of PVA and NaCl in the model fluids, which are of higher concentrations than copper salt, make it difficult to differentiate their copper content by mapping techniques based on elemental contrast. Therefore, a fluorometric detector mechanism was developed, which is inspired by our earlier work of fluorescence quenching microscopy (FQM).[42,43] As shown in Figure 10A, the detector film is now a fluorescence dye/polymer layer spin-coated on a glass substrate. Neocuproine (Nc) is often used in quantitative analysis of copper content in solution based on colorimetric response.[44] Unfortunately, direct colorimetric response from the molecular dye was too weak to generate sufficient contrast in optical images. Alternatively, the fluorescence of Nc, which can be quenched in the presence of Cu^{2+} (see Figure S7), is employed for microscopy imaging. Under fluorescence mode, droplets modified with Cu should generate dark spots on a bright background due to fluorescence quenching, while unmodified droplets should not. Figure 10B is an FQM image showing the dry marks of unmodified droplets sprayed through a pristine gauze without any modifiers. Although the dry marks are slightly visible, they do not quench the fluorescence. Figure 10C is an FQM image of the dry marks of copper-modified droplets sprayed directly from Cu-containing model fluid. Indeed, all the droplets appear as dark spots. By comparing the contrasts of these dark spots with those generated from droplets with known copper concentrations (Figure S8), one can conclude that the concentration of Cu^{2+} in the modified droplets

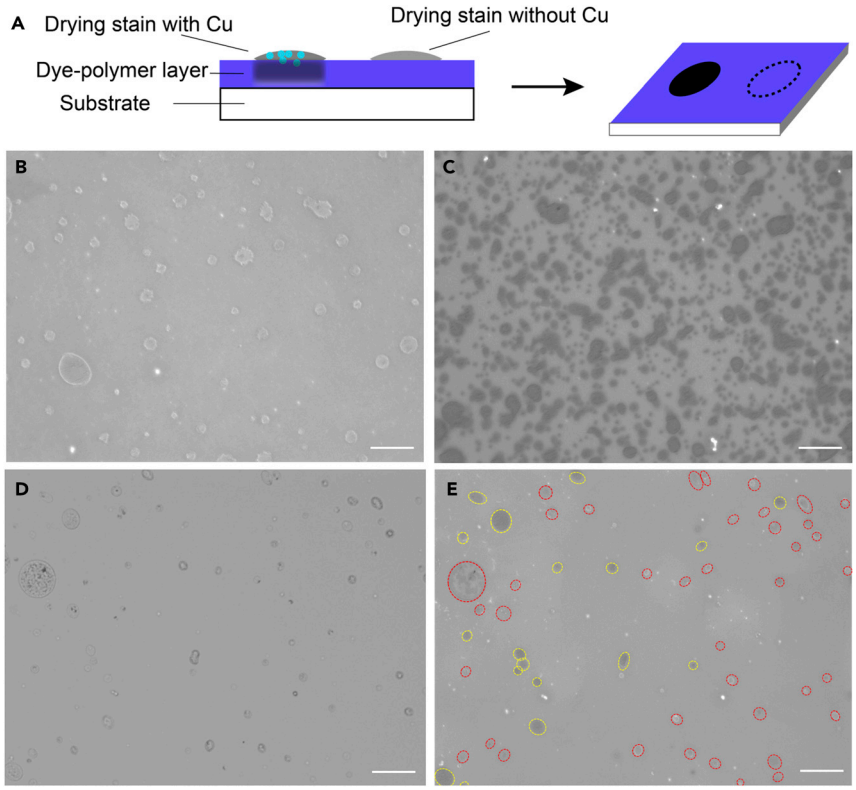

Figure 10. Modulation of Droplets by Cu Ions and Fluorometric Visualization

(A) Droplets passing through polyaniline-coated fabrics doped with $CuSO_4$ can dissolve Cu ions. A Nc/PMMA film spin-coated on a coverglass was used as a fluorometric detector to capture the droplets, which was then imaged by FQM. The Cu-modified droplets can quench the fluorescence of their underlying Nc dye and thus appear as dark spots under FQM.

(B) Fluorescence image of a control sample of Cu-free droplets on the detector film, showing drying marks of droplets, which did not quench the fluorescence.

(C) Fluorescence image of another control sample of Cu-containing droplets on the detector film. The stains quenched fluorescence strongly and appeared as dark spots.

(D) Transmission mode of image of a sample collected after they passed a Cu-loaded gauze, which clearly shows the drying marks of the droplets, but cannot differentiate which droplets were modified with Cu.

(E) Under fluorescence mode, Cu-modified droplets are clearly visible as dark spots. The yellow circles highlight modified droplets and the red circles mark the unmodified ones. A total of 18 out of 58 droplets were modified. All scale bars represent 50 μm.

is $>10^{-4}$ M, which is above the threshold needed for deactivating influenza viruses.[45] Note that the concentration of copper can become even higher as these droplets dry and shrink further.

Gauze cloths coated with polyaniline doped with $CuSO_4$ were tested in the same way as shown in Figure 2B. Droplets collected and dried on the detector film were imaged under both transmission (Figure 10D) and fluorescence (Figure 10E) modes. In the transmission mode, all droplet marks are visible. In FQM mode, Cu-containing droplets can be differentiated by their characteristic dark appearance. In Figure 10E, modified and unmodified droplets are circled by red and yellows lines, respectively. By visual observation, 18 out of 58 spots appear dark, suggesting a η_n of 31%. Note that this is higher than the η_n for H_3PO_4 due to the much more conservative threshold to categorize modified droplets.

Control Experiments Simulating Inhalation

The results shown above demonstrate the promise of using a chemical modifying layer to contaminate outgoing respiratory droplets with soluble molecular species for the purpose of inactivating released pathogens. This may help to enhance public health response to reduce the spread of infectious respiratory diseases. Since people also inhale air through face covers, it is crucial to avoid the release of particles or chemicals from the modifying layer. As illustrated in Figure 2A, one of the major differences between exhalation and inhalation is the presence of droplets. Ambient air without droplets should not trigger the release. Therefore, volatile species or nanoparticle-based droplet modifiers were intentionally avoided due to the potential risk of desorption or detachment, which could lead to direct delivery into the respiratory tracts or even the lungs through inhalation. Therefore, the selection of antipathogen agents is narrowed down to nonvolatile and water-soluble species, as they can be selectively dissolved by droplets but not released in air flow.

Indeed, passing ambient air through a dry, unused Cu-loaded fabric releases a barely detectable level of copper ions in the downstream air (see Supplemental Information). However, in practice a nonwoven fabric can often be dampened when entrapped respiratory droplets accumulate, which increases the humidify of inhaled air. It is also important that the mask modifiers should not be readily released in high-humidity air or through a damp mask during normal inhalation. Therefore, control experiments simulating harsher and wetter inhalation conditions were carried out to examine whether copper ions or acids can be released from the polyaniline-coated fibers. As illustrated in Figure S9, high-humidity air (23°C, 99% relative humidity) was drawn through a lint-free wipe sandwiched between two chambers, one of which was connected to a house vacuum. The wipe was first dampened by spraying the model respiratory liquid for 1 s to simulate accumulated entrapped fluid. Two air-flow speeds (0.2 m/s and 1 m/s) comparable with the low and high ends of typical rates of inhalation were tested. The air "inhaled" through the $CuSO_4$- or H_3PO_4-loaded wipe was then bubbled through a 10-mL deionized water reservoir to dissolve any released copper salt or acid. After 1 h of continuous "inhalation," the concentrations of copper and proton in the 10-mL water reservoir were measured by inductively coupled plasma mass spectrometry (ICP-MS) and a pH meter, respectively. The results (Figure S9 and Table S3) showed no significant increase in the proton or copper concentration in the reservoir, even when the wipe was subjected to an extreme air-flow rate of 6 m/s for 10 min. For all the flow rates tested, the copper concentrations in the reservoir were below the mean level in natural water, and orders of magnitude lower than the upper limit of copper contaminant level in drinkable water.[46]

Conclusion and Outlook

Due to the limited experimental capabilities, the droplets characterized in this work are mostly larger than 10 μm in diameter. Note that these large droplets should make up a significant majority in the overall volume of respiratory fluids released in expiratory activities. Although these droplets usually settle down easily, they contain high loadings of viruses due to their larger volumes, turning objects into infectious fomites. They can also turn into smaller-sized nuclei after evaporation,[47–49] which may stay suspended in air flow for an extended period of time. Viruses in the nuclei are surrounded and protected by a myriad of other respiratory masses and could stay infectious for a long time. An on-mask chemical modulation strategy could help to reduce the viability of viruses and other pathogens of infectious respiratory diseases released from patients.

Nonwoven fabrics are known to be effective in trapping droplets, and here we show that they are also an effective material platform for chemically modulating respiratory droplets. Low packing density (11%) fabric such as a medical gauze does not cause measurable pressure drop, but can readily modify 19% of the escaped droplet by number and 28% by volume. Increasing the fiber density to 19% leads to 49% of outgoing droplets being modified by number and 82% by volume. In practice, the modulation layer can be applied as an add-on at the outer surface of the common masks or as an insert. Although polyaniline is used as a model coating material here, it does offer an additional benefit in that it changes color when acid or metal ions are depleted from the modifying layer. Depleted coatings can also be easily regenerated by redoping (Figure S10). It is worth noting that there should be many other combinations of antipathogen molecules (e.g., quaternary ammonium compounds) and polymer coatings (e.g., sulfonated polyaniline, poly(styrene sulfonate), and polypeptides) suitable for achieving droplet modification, as long as they do not easily desorb or detach during inhalation. The polymer should be able to reversibly load and release those chemical modifier compounds and must strongly adhere to the nonwoven fabrics, which may be achieved by covalent grafting or even being directly incorporated as a component in the fibers.

A mask blocks and interacts with particulate matter in both incoming and outgoing directions. Thus, it offers protection for both the wearer and other people around the wearer, the latter of which turns out to be crucial in the public health response to the current COVID-19 pandemic and has been mandated in many regions. In this regard, a mask is not only "personal protective" equipment, but more importantly "public heath" equipment. The work presented here highlights this aspect of mask wearing and enhances its protection function of others around potential carriers.[8,] Much work remains to be done to make this on-mask chemical modulation approach a disease-control tool for public health. It may also be useful for better protecting heathcare workers in patient wards or those large temporary shelter hospitals for triaging, isolating, and caring for patients with non-critical conditions.[50] We believe it is a worthwhile effort because reducing the infectiousness of the sources cuts down direct person-to-person transmission, reduces indirect transmission through fomites, and lowers the burden of other measures along the transmission pathways of infectious respiratory diseases.

EXPERIMENTAL PROCEDURES

Resource Availability

Lead Contact

Further information and requests for resources and reagents should be directed to and will be fulfilled by the Lead Contact, Jiaxing Huang (jiaxing-huang@northwestern.edu).

Materials Availability

This study did not generate new unique reagents.

Data and Code Availability

Source data and MATLAB codes for figures in the paper are available upon request.

Preparation of Chemical Modulation Layer

In a typical experiment, a piece of nonwoven fabric with a width of 5 cm and a length of 60 cm was immersed in a premixed solution of 5 mL of aniline in 30 mL of 1 M HCl. The fabric was manually rubbed to remove the bubble and ensure wetting. Ammonium persulfate (APS; 0.5 g) was dissolved in 30 mL of 1 M HCl and added into the

aniline solution after a few minutes. The mixture was rubbed and stirred slightly by hand and left with sealing overnight. The color of the fabric usually started to darken after a few minutes. The next day, the fabric was rinsed with deionized water three times to remove by-products and loosely bonded polyaniline. Before doping with acids or copper salts, the fabric was squeezed to remove water and tap dried with paper towels. It was then immersed in phosphoric acid solution (pH 1) for 30 min, followed by rinsing in ethyl alcohol twice to remove the excessive acid solution. For copper treatment, instead of acids, the coated fabric was put into 0.1 M $CuSO_4$ solution for 30 min and washed with ethyl alcohol. After drying in air, the fabric was blown with ambient air at about 20 m/s for 30 s using an air sprayer (Paasche, VLS0316) without loading any fluid to further remove weakly bonded polyaniline, if any. All chemicals were purchased from Sigma-Aldrich. The medical gauzes were purchased from Walgreens (premium rolled gauze, item code 150014). Lint-free wipes were purchased from Fisher Scientific (Technicloth #TX606). See Table S4 for detailed information of the fabrics.

Preparation of Colorimetric Detector Film

Aniline (0.5 mL) was dissolved in 20 mL of 1 M HCl solution. APS (0.5 g) was dissolved in another 20 mL of 1 M HCl solution. The two solutions were mixed under stirring. The substrate (Celgard Li-ion battery separator film), typically 5 cm × 5 cm, was immediately put on the surface of the solution with continuous stirring. Caution was taken to avoid trapping air bubbles underneath the film. After 20 min, the green film was removed from the solution and rinsed in deionized water. After drying it was placed on the surface of 0.1 wt % of ammonia solution for 30 min to be dedoped. Finally, it was rinsed with ethyl alcohol to remove excess ammonia solution.

Preparation of Model Respiratory Fluid

PVA with a molecular weight of 143,000 was dissolved in water at 80°C and 2.5 mg/mL. NaCl was then added to the solution after cooling to room temperature at a concentration of 10 mg/mL. Model fluid with known pH was made by adding a known volume of phosphoric acid into PVA/NaCl solution. The pH was further confirmed by a pH meter (Fisher Scientific AE150). PVA and NaCl were purchased from Sigma-Aldrich.

Preparation of Fluorometric Detector Film

Poly(methyl methacrylate) (PMMA; molecular weight ~350,000) at a concentration of 10 mg/mL was dissolved in anisole, followed by dissolving neocuproine hemihydrate (99%) at a concentration of 25 mg/mL. The solution was spin-coated on a coverglass by a spin coater (model #WS-400BZ-6NPP/LITE, Laurell Technologies, North Wales, PA, USA) at 2,000 rpm for 1 min. The chemicals were purchased from Sigma-Aldrich.

Simulation of Coughing and Sneezing

An air sprayer (Paasche, VLS0316) was connected to an air compressor set to 40 psi. A solenoid valve with a working voltage of 12 V was placed at the outlet of the compressor and also connected to a programmable source meter (Tekpower TP3005P), which was connected to a laptop computer. Spraying time was controlled by setting the duration of voltage output. The flux of the sprayer was adjusted so that 1 s of spraying yielded a sufficient number of droplets on the detection screen. A home-made channel was used to fix the fabric and the detection screen. The sprayer was placed 2 cm away from the fabric and pointed to it to simulate the situation of a person wearing a mask. The sprayed area on the fabric was approximately 2.5 cm × 2.5 cm. For lint-free wipes with lower penetrating rate, the distance was adjusted to

0.5 cm to increase the flux so that enough droplets could be received on the screen. The distance from the fabric layer to the detection film was 4 cm for both cases. For each spraying test, the time was set to 1 s. Longer spraying time would lead to water-layer formation on the fabric and bias the result. The fabric was dried in air before the next spray. Each fabric was sprayed three times at the same spot. The detection screen was cut to a size of 2 cm × 2 cm to receive escaped droplets.

Optical Microscopy

All detection screens were examined a few minutes after spraying using an optical microscope (Nikon Eclipse E600 POL upright microscope; Nikon Instruments, Melville, NY, USA) equipped with a CCD camera (2,048 × 1,536 pixels; Teledyne QImaging, MicroPublisher 3.3 RTV, Surrey, BC, Canada) under reflection (bright-field) and transmission mode (dark-field). Offset, exposure time, and gain of the camera were to set to 0, 40 ms, and 2.56, respectively. Regions with sparse droplets or dirty background were discarded.

Fluorescence Quenching Microscopy

FQM images were taken on a Nikon Eclipse TE2000-U inverted fluorescence microscope (Nikon Instruments) equipped with an X-cite 120 PC illumination system (EXFO Photonic Solutions, Mississauga, ON, Canada) as the light source. An ET-GFP filter cube (FITC/Cy2; Chroma Technology, Bellows Falls, VT, USA) was used to select light in the UV range. Exposure time was 10 s.

Characterization Methods

SEM images were obtained by a field-emission scanning electron microscope (SU8300; Hitachi). The thickness of colorimetric detection layer was measured using an atomic force microscope (XE-100; Park Systems) under non-contact mode. Elemental analysis was conducted on a Thermo iCAP Q inductively coupled plasma mass spectrometer.

Control Experiment Simulating Inhalation

Cu-loaded lint-free wipes and acid-loaded wipes were sprayed by model respiratory fluid for 1 s to simulate dampened fabrics. An ultrasonic humidifier was used to create highly humid upstream air (99% relative humidity), which was drawn through the wipes at air-flow speeds of 0.2 m/s and 1 m/s for 1 h. The downstream air was then guided into a tube containing 10 mL of deionized water. The same process was repeated at an extreme flow rate of 6 m/s for 10 min. The concentration of Cu and protons from the masking layer in the deionized water reservoir were analyzed by ICP-MS and a pH meter (Fisher Scientific AE150). See Supplemental Information for more details.

Image Processing

Readers are referred to Supplemental Information for detailed processes.

SUPPLEMENTAL INFORMATION

Supplemental Information can be found online at https://doi.org/10.1016/j.matt.2020.10.012.

ACKNOWLEDGMENTS

The work is mainly supported by a National Science Foundation (RAPID DMR-2026944 managed by SSMC subdivision). H.H. thanks the Ryan Fellowship and the Northwestern University International Institute for Nanotechnology for encouragement. Y.L. thanks his parents for funding his study at Northwestern University.

Additional sources of support include Dean's support from the McCormick School of Engineering to support J.H. and an earlier gift donation to J.H.'s lab, and personal donations from some of the authors in purchasing small supplies and consumables to expedite the work. The work made use of the IMSERC and the Keck-II facility of the NUANCE Center at Northwestern University, which has received support from the NSF (CHE-1048773); Soft and Hybrid Nanotechnology Experimental Resource (NSF ECCS-1542205); the MRSEC program (NSF DMR-1720139) at the Materials Research Center; the Keck Foundation; the State of Illinois and International Institute for Nanotechnology. The authors also thank Profs. L. Jiang (Beijing), Q. Cheng (Beijing), and W. Zhang (Nanjing), and Ms. X. Xiao (Chicago) for their gifts of various types of masks and supplies, some of which were used to better equip the authors to perform on-site research during the period of stay-home order of the State of Illinois, and Dr. M. Kadir, Dr. Z. Yu, L. Prestowitz, L.J. Bichelmeir, S.G. Fine, Mr. J. Suerth (Feynlab), and many others for helpful discussions and encouragement.

AUTHOR CONTRIBUTIONS

J.H. conceptualized the work and oversaw the research. H.H. and H.P. designed the experiments, developed the colorimetric and fluorometric detection methods, and drafted the manuscript. H.H. and Y.L. designed the image-processing protocol; Y.L. wrote the codes to extract and analyze data from the optical microscopy images.

DECLARATION OF INTERESTS

Northwestern University has filed a patent application including discoveries made in this work.

Received: August 7, 2020
Revised: September 30, 2020
Accepted: October 7, 2020
Published: October 29, 2020

REFERENCES

1. Gates, B. (2020). Responding to Covid-19—a once-in-a-century pandemic? N. Engl. J. Med. *382*, 1677–1679.

2. Huang, H., Fan, C., Li, M., Nie, H.-L., Wang, F.-B., Wang, H., Wang, R., Xia, J., Zheng, X., Zuo, X., et al. (2020). COVID-19: a call for physical scientists and engineers. ACS Nano *14*, 3747–3754.

3. Flint, J., Racaniello, V.R., Rall, G.F., and Skalka, A.M. (2015). Principles of Virology (John Wiley & Sons).

4. Siegel, J.D., Rhinehart, E., Jackson, M., Chiarello, L., and Practices, H.C.I.C. (2007). 2007 guideline for isolation precautions: preventing transmission of infectious agents in health care settings. Am. J. Infect. Control *35*, S65–S164.

5. World Health Organization. Transmission of SARS-CoV-2: Implications for Infection Prevention Precautions. https://www.who.int/publications/i/item/modes-of-transmission-of-virus-causing-covid-19-implications-for-ipc-precaution-recommendations.

6. Xie, X., Li, Y., Sun, H., and Liu, L. (2009). Exhaled droplets due to talking and coughing. J. R. Soc. Interfaces *6* (*Suppl 6*), S703–S714.

7. Mittal, R., Ni, R., and Seo, J.-H. (2020). The flow physics of COVID-19. J. Fluid Mech. *894*, F2.

8. Leung, N.H.L., Chu, D.K.W., Shiu, E.Y.C., Chan, K.H., McDevitt, J.J., Hau, B.J.P., Yen, H.L., Li, Y., Ip, D.K.M., Peiris, J.S.M., et al. (2020). Respiratory virus shedding in exhaled breath and efficacy of face masks. Nat. Med. *26*, 676–680.

9. Scharfman, B.E., Techet, A.H., Bush, J.W.M., and Bourouiba, L. (2016). Visualization of sneeze ejecta: steps of fluid fragmentation leading to respiratory droplets. Exp. Fluids *57*, 24.

10. Han, Z.Y., Weng, W.G., and Huang, Q.Y. (2013). Characterizations of particle size distribution of the droplets exhaled by sneeze. J. R. Soc. Interfaces *10*, 20130560.

11. Bourouiba, L., Dehandschoewercker, E., and Bush, J.W.M. (2014). Violent expiratory events: on coughing and sneezing. J. Fluid Mech. *745*, 537–563.

12. Cook, T.M. (2020). Personal protective equipment during the coronavirus disease (COVID) 2019 pandemic—a narrative review. Anaesthesia *75*, 920–927.

13. Li, X.P., Niu, J.L., and Gao, N.P. (2012). Characteristics of physical blocking on co-occupant's exposure to respiratory droplet residuals. J. Cent. South Univ. *19*, 645–650.

14. Verma, S., Dhanak, M., and Frankenfield, J. (2020). Visualizing the effectiveness of face masks in obstructing respiratory jets. Phys. Fluids (1994) *32*, 061708.

15. Centers for Disease Control and Prevention. CDC Calls on Americans to Wear Masks to Prevent COVID-19 Spread. https://www.cdc.gov/media/releases/2020/p0714-americans-to-wear-masks.html.

16. Konda, A., Prakash, A., Moss, G.A., Schmoldt, M., Grant, G.D., and Guha, S. (2020). Aerosol filtration efficiency of common fabrics used in respiratory cloth masks. ACS Nano *14*, 6339–6347.

17. Zhao, M., Liao, L., Xiao, W., Yu, X.Z., Wang, H.T., Wang, Q.Q., Lin, Y.L., Kilinc-Balci, F.S., Price, A., Chu, L., et al. (2020). Household materials selection for homemade cloth face coverings and their filtration efficiency enhancement with triboelectric charging. Nano Lett. *20*, 5544–5552.

18. Roberge, R.J. (2008). Effect of surgical masks worn concurrently over N95 filtering facepiece

respirators: extended service life versus increased user burden. J. Public Health Manag. Pract. *14*, E19–E26.

19. Lee, J.H., Wu, C.Y., Lee, C.N., Anwar, D., Wysocki, K.M., Lundgren, D.A., Farrah, S., Wander, J., and Heimbuch, B.K. (2009). Assessment of iodine-treated filter media for removal and inactivation of MS2 bacteriophage aerosols. J. Appl. Microbiol. *107*, 1912–1923.

20. Quan, F.S., Rubino, I., Lee, S.H., Koch, B., and Choi, H.J. (2017). Universal and reusable virus deactivation system for respiratory protection. Sci. Rep. *7*, 39956.

21. Si, Y., Zhang, Z., Wu, W., Fu, Q., Huang, K., Nitin, N., Ding, B., and Sun, G. (2018). Daylight-driven rechargeable antibacterial and antiviral nanofibrous membranes for bioprotective applications. Sci. Adv. *4*, eaar5931.

22. Liu, H., Cao, C.Y., Huang, J.Y., Chen, Z., Chen, G.Q., and Lai, Y.K. (2020). Progress on particulate matter filtration technology: basic concepts, advanced materials, and performances. Nanoscale *12*, 437–453.

23. Rubino, I., and Choi, H.J. (2017). Respiratory protection against pandemic and epidemic diseases. Trends Biotechnol. *35*, 907–910.

24. Zhou, J., Hu, Z., Zabihi, F., Chen, Z., and Zhu, M. (2020). Progress and perspective of antiviral protective material. Adv. Fiber Mater. *2*, 123–139.

25. Balagna, C., Perero, S., Percivalle, E., Nepita, E.V., and Ferraris, M. (2020). Virucidal effect against coronavirus SARS-CoV-2 of a silver nanocluster/silica composite sputtered coating. Open Ceram. *1*, 100006.

26. Darnell, M.E., Subbarao, K., Feinstone, S.M., and Taylor, D.R. (2004). Inactivation of the coronavirus that induces severe acute respiratory syndrome, SARS-CoV. J. Virol. Methods *121*, 85–91.

27. Scheller, C., Krebs, F., Minkner, R., Astner, I., Gil-Moles, M., and Watzig, H. (2020). Physicochemical properties of SARS-CoV-2 for drug targeting, virus inactivation and attenuation, vaccine formulation and quality control. Electrophoresis *41*, 1137–1151.

28. Vincent, M., Hartemann, P., and Engels-Deutsch, M. (2016). Antimicrobial applications of copper. Int. J. Hyg. Environ. Health *219*, 585–591.

29. Mitra, D., Kang, E.T., and Neoh, K.G. (2020). Antimicrobial copper-based materials and coatings: potential multifaceted biomedical applications. ACS Appl. Mater. Interfaces *12*, 21159–21182.

30. Dimitriev, O.P. (2004). Doping of polyaniline by transition-metal salts. Macromolecules *37*, 3388–3395.

31. Huang, J.X. (2006). Syntheses and applications of conducting polymer polyaniline nanofibers. Pure Appl. Chem. *78*, 15–27.

32. Virji, S., Fowler, J.D., Baker, C.O., Huang, J., Kaner, R.B., and Weiller, B.H. (2005). Polyaniline nanofiber composites with metal salts: chemical sensors for hydrogen sulfide. Small *1*, 624–627.

33. Chiang, J.C., and Macdiarmid, A.G. (1986). Polyaniline-protonic acid doping of the emeraldine form to the metallic regime. Synth. Met. *13*, 193–205.

34. Vejerano, E.P., and Marr, L.C. (2018). Physico-chemical characteristics of evaporating respiratory fluid droplets. J. R. Soc. Interface *15*, 20170939.

35. Yang, W., Elankumaran, S., and Marr, L.C. (2012). Relationship between humidity and influenza A viability in droplets and implications for influenza's seasonality. PLoS One *7*, e46789.

36. Li, D., Huang, J.X., and Kaner, R.B. (2009). Polyaniline nanofibers: a unique polymer nanostructure for versatile applications. Acc. Chem. Res. *42*, 135–145.

37. Gralton, J., Tovey, E., McLaws, M.L., and Rawlinson, W.D. (2011). The role of particle size in aerosolised pathogen transmission: a review. J. Infect. *62*, 1–13.

38. Kimme, C., Ballard, D., and Sklansky, J. (1975). Finding circles by an array of accumulators. Commun. ACM *18*, 120–122.

39. Jin, Z., Su, Y.X., and Duan, Y.X. (2000). An improved optical pH sensor based on polyaniline. Sens. Actuators B *71*, 118–122.

40. Zhang, R.F., Liu, B.F., Yang, A.K., Zhu, Y.Y., Liu, C., Zhou, G.M., Sun, J., Hsu, P.C., Zhao, W.T., Lin, D.C., et al. (2018). In situ investigation on the nanoscale capture and evolution of aerosols on nanofibers. Nano Lett. *18*, 1130–1138.

41. Gac, J.M., and Gradon, L. (2012). Analytical investigation and numerical modeling of collisions between a droplet and a fiber. J. Colloid Interface Sci. *369*, 419–425.

42. Kim, J., Cote, L.J., Kim, F., and Huang, J.X. (2010). Visualizing graphene based sheets by fluorescence quenching microscopy. J. Am. Chem. Soc. *132*, 260–267.

43. Kong, Z.Z., Daab, M., Yano, H., Huang, H.Y., Breu, J., Sasaki, T., Nguyen, S.T., and Huang, J.X. (2020). Visualizing transparent 2D sheets by fluorescence quenching microscopy. Small Methods *4*, 2000036.

44. Larsen, E.R. (1974). Spectrophotometric determination of copper in fertilizer with neocuproine. Anal. Chem. *46*, 1131–1132.

45. Imai, K., Ogawa, H., Bui, V.N., Inoue, H., Fukuda, J., Ohba, M., Yamamoto, Y., and Nakamura, K. (2012). Inactivation of high and low pathogenic avian influenza virus H5 subtypes by copper ions incorporated in zeolite-textile materials. Antivir. Res. *93*, 225–233.

46. Gaetke, L.M., and Chow, C.K. (2003). Copper toxicity, oxidative stress, and antioxidant nutrients. Toxicology *189*, 147–163.

47. Stadnytskyi, V., Bax, C.E., Bax, A., and Anfinrud, P. (2020). The airborne lifetime of small speech droplets and their potential importance in SARS-CoV-2 transmission. Proc. Natl. Acad. Sci. U S A *117*, 11875–11877.

48. Weber, T.P., and Stilianakis, N.I. (2008). Inactivation of influenza A viruses in the environment and modes of transmission: a critical review. J. Infect. *57*, 361–373.

49. Liu, L., Wei, J., Li, Y., and Ooi, A. (2017). Evaporation and dispersion of respiratory droplets from coughing. Indoor Air *27*, 179–190.

50. Zhang, Z., Chen, S., Yang, J., Wang, J., Zhai, X., Barnighausen, T., et al. (2020). Fangcang shelter hospitals: a novel concept for responding to public health emergencies. Lancet *395*, 1305–1314.

Matter, Volume *3*

Supplemental Information

On-Mask Chemical Modulation of Respiratory Droplets

Haiyue Huang, Hun Park, Yihan Liu, and Jiaxing Huang

Supplemental Data

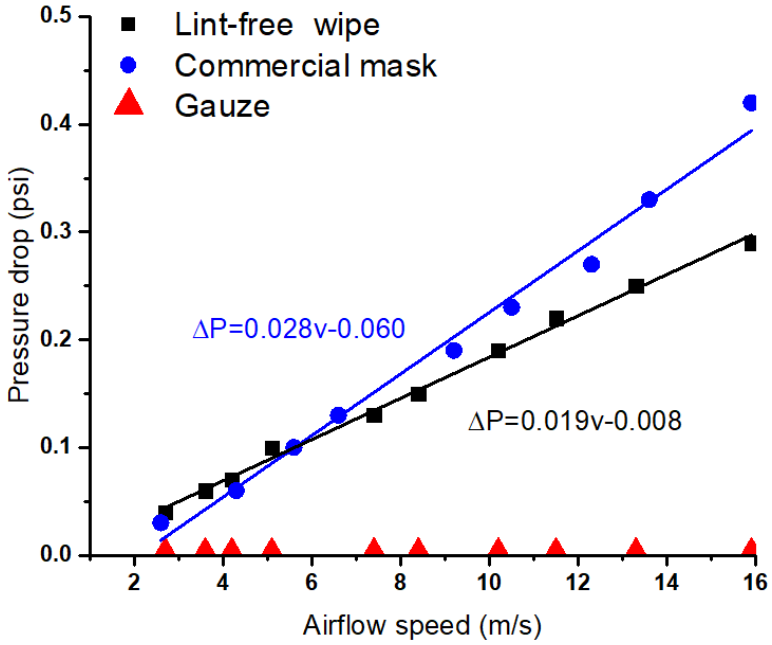

Fig. S1 Pressure drop across different fabrics at different airflow speeds. The pressure drop of gauze was below the measuring limit. The commercial mask sample refers to a typical medical mask with a dense middle layer of melt-spun polypropylene fiber mat.

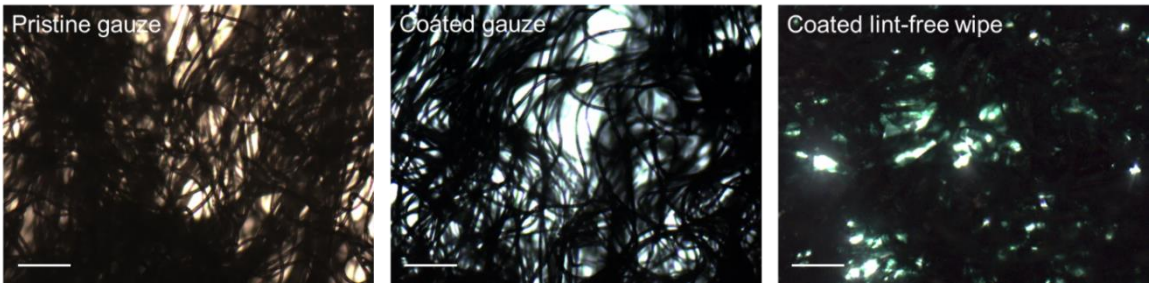

Fig. S2 Optical microscopic images under transmission mode for a pristine gauze (left), a coated gauze (middle), and a coated lint-free wipe (right), respectively. The gauze is less densely packed compared to the lint-free wipe. Scale bars are 200 μm.

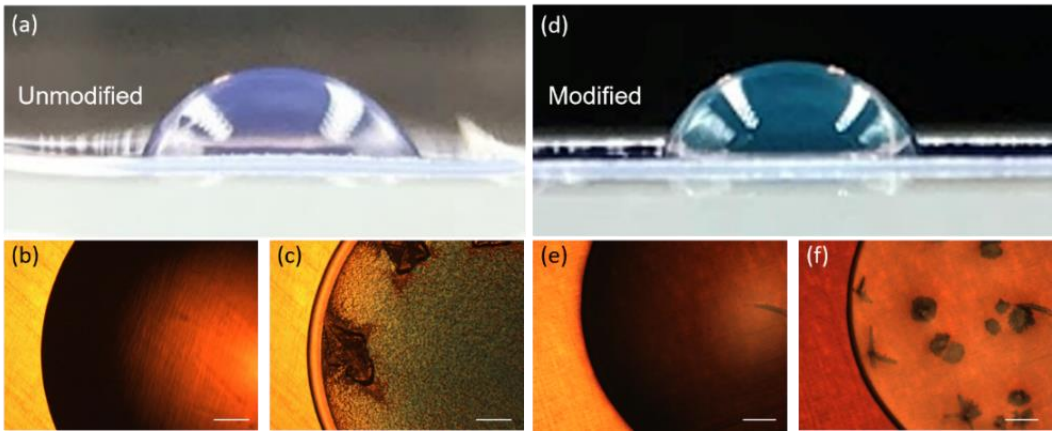

Fig. S3 Observation of contact angle and contact line of droplets on polyaniline detector film. Side view of a 10-μL droplet of (a) unmodified and (d) modified model fluid on polyaniline coated detector film, showing similar contact angles. Top view of 2 μL of unmodified droplet, (b) before and (c) after drying, showing that the initial contact line becomes the edge of the final dried stain. (e-f) This is also observed for an acid modified droplet. All scale bars are 200 μm.

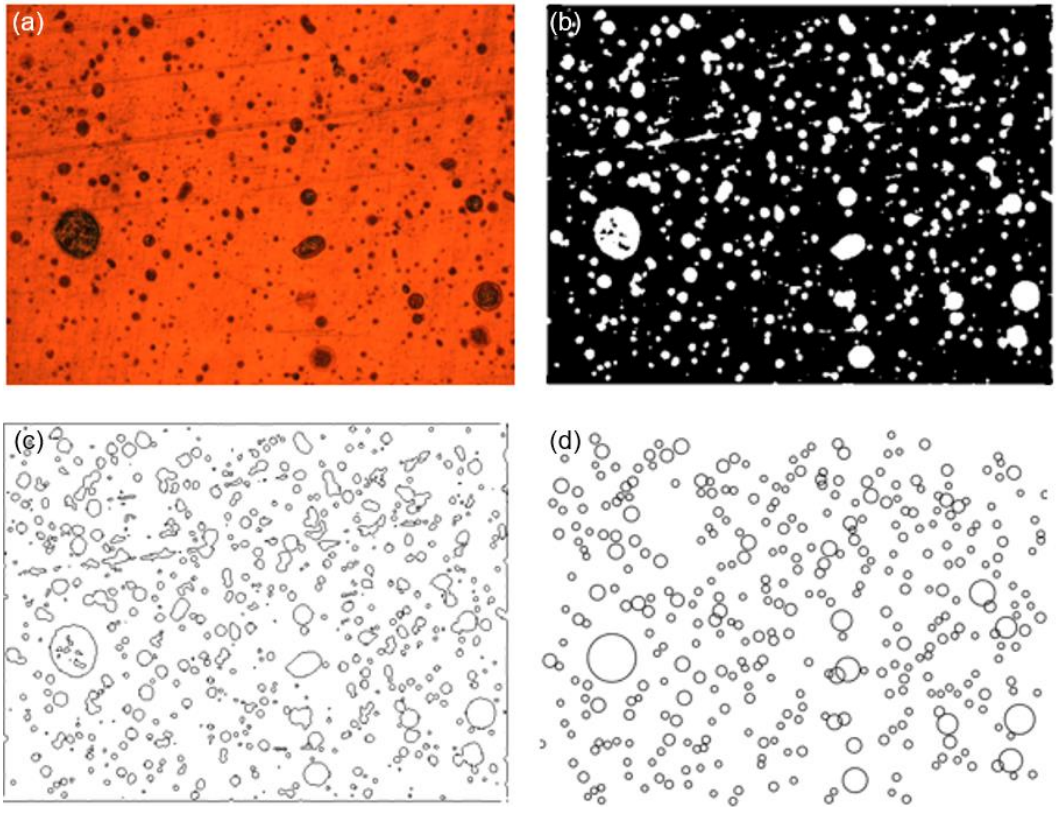

Fig. S4 Hough circle transformation removes unwanted features from (a) the raw image taken under reflection mode, such as the lines of rolling mark on the plastic film. (b) Pre-processing steps are then performed to convert it to a binarized image with reduced noise and inversed contrast. (c) If directly converted to outlines, artifacts associated with the rolling mark are also included. (d) With Hough circle transformation, droplets are approximated as circles and those high-aspect-ratio artifacts are removed, improving the overall accuracy of recognizing droplets.

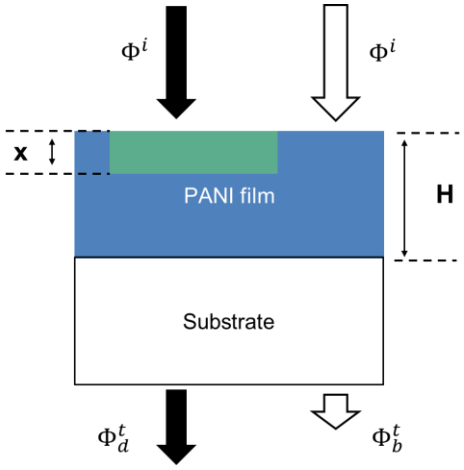

Fig. S5 Parameters used to calculate contrast in transmission images. The doped range of polyaniline (*i.e.*, stain of a modified droplet) was approximated as a cylinder with thickness of *x*. The total thickness of the polyaniline layer is *H*. Φ^i is the intensity of incident light, Φ^t_d is the intensity of transmitted light for a pixel inside a droplet, Φ^t_b is the intensity of transmitted light for a pixel belonging to the background.

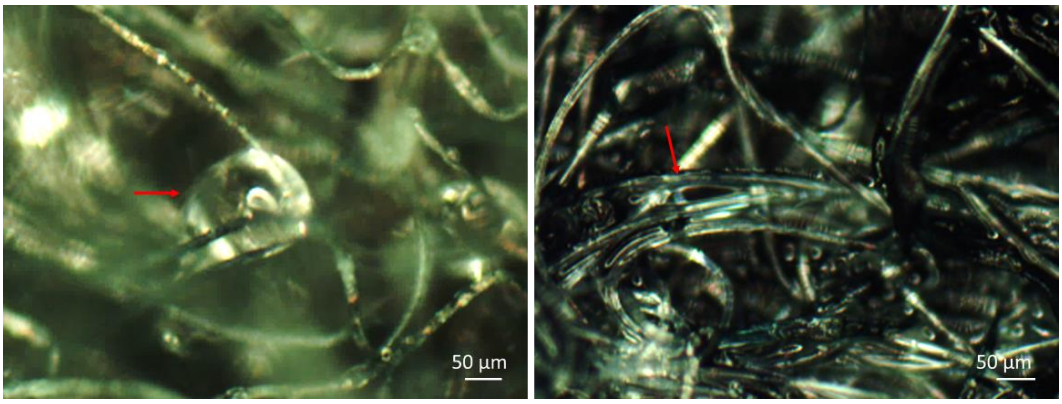

Fig. S6 Optical microscopy images (reflective mode, dark field) of a polyaniline-coated gauze (left) and wipe (right) immediately after spraying. As indicated by the red arrows, large droplets and even liquid films can be observed trapped between fibers.

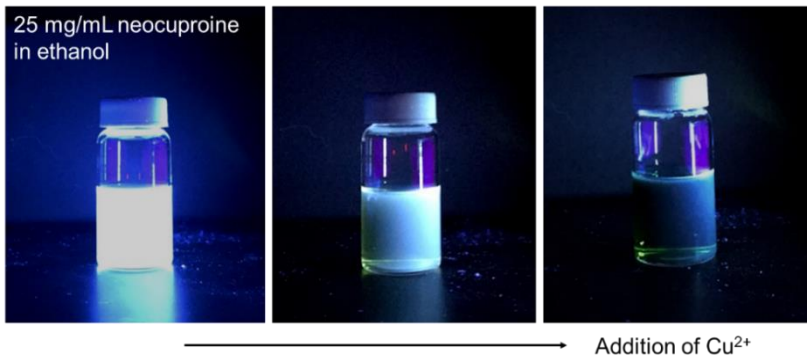

Fig. S7 Quenching of neocuproine's (Nc) fluorescence by Cu^{2+}. The fluorescence of Nc was excited by a UV lamp placed outside the image, which irradiated the sample from the right side. With the addition of $CuSO_4$, the fluorescence was clearly quenched. This inspires the use of Nc dye in fluorescence quenching microscopy to image Cu-modified droplets.

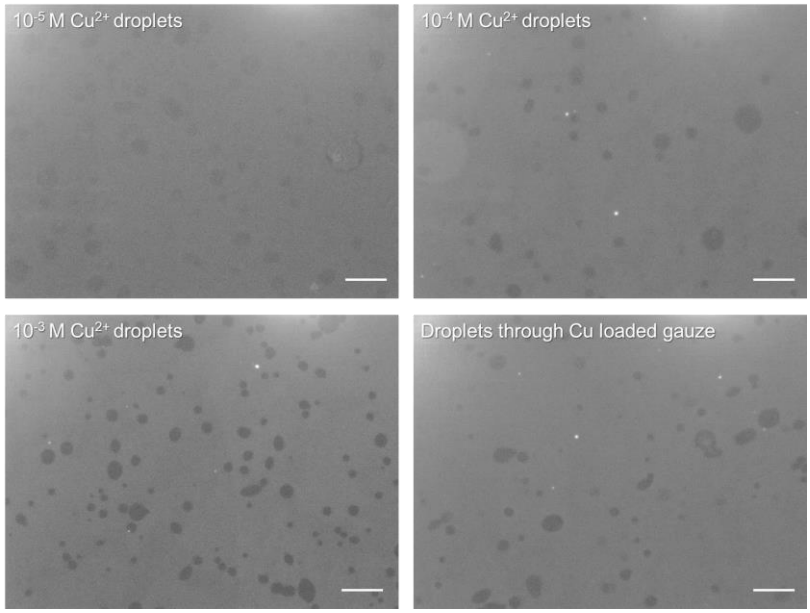

Fig. S8 Fluorescence quenching microscopic images for drying stains of droplets with different concentrations of Cu^{2+}. Model respiratory fluid with different concentrations of Cu^{2+} (10^{-5} to 10^{-3} M) were sprayed to the fluorometric detector films. Stains of the droplets start to show clear contrast against the background when the Cu concentration is larger than 10^{-4} M. An image for droplets passing through a Cu-loaded gauze is also included (obtained under the same condition as **Fig. 10e**), indicating modified droplets have a Cu concentration of at least >10^{-4} M. All scale bars are 50 μm.

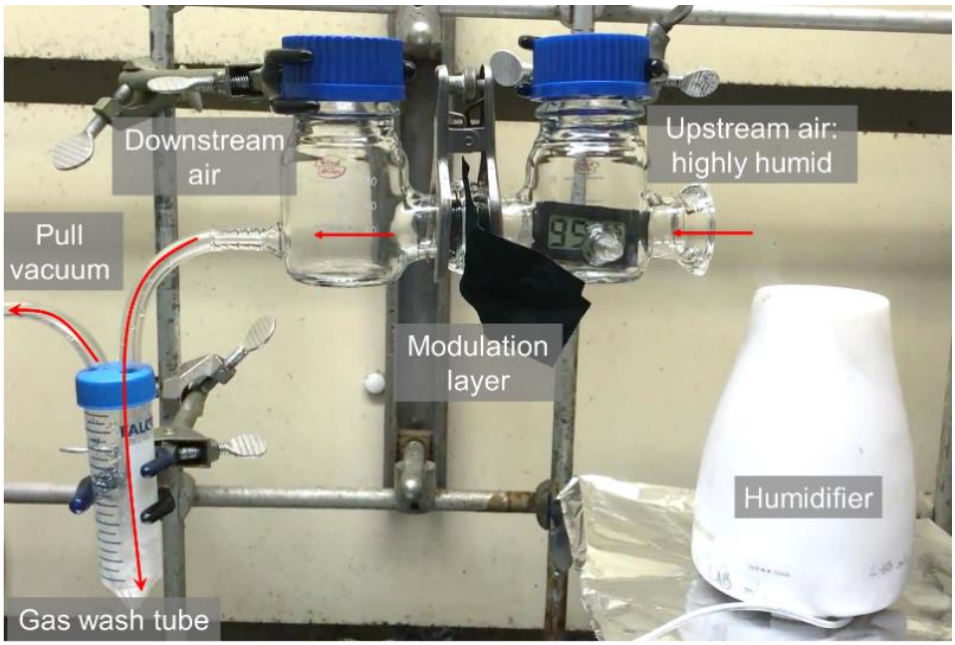

Fig. S9 Experimental setup to simulate inhalation of humid air through a damp fabric. An ultrasonic humidifier was used to generate 99% relative humidity (RH) in the upstream air (measured by a sensor inside the upstream chamber), which was drawn through the lint-free wipe loaded with copper ions or acids. The wipe was sandwiched between two chambers, one of which was connected to the house vacuum. The downstream air was then guided to a tube and bubbled through 10 mL of deionized water reservoir to dissolve released copper ions or acids, if any. No condensation of water was observed in the downstream chamber for all these flow rates. A valve (not shown) was used to control the airflow rate.

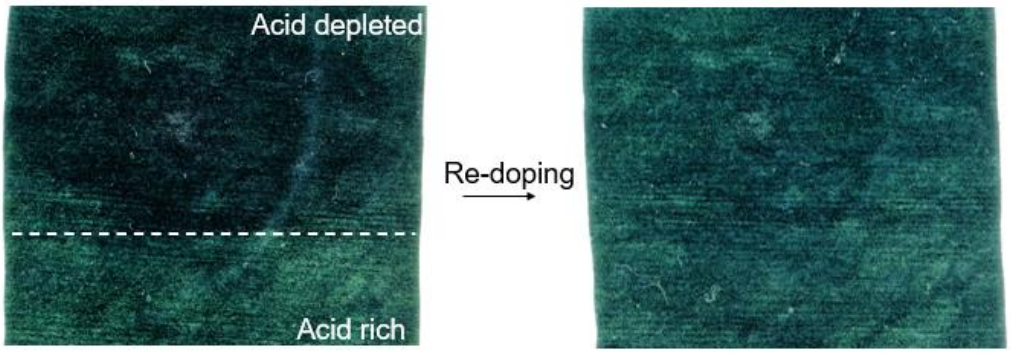

Fig. S10 Acid-depleted area of the polyaniline-coated gauze appears darker than the acid-rich area, giving a visual indicator for replacement or reloading acid (or copper ions).

Table S1. Experimental conditions used in this work in comparison to real expiratory human activities. Data were adapted from references[1-3].

	Sneezing	Coughing	Our experiment
Airflow speed	Up to 30-100 m/s		20 m/s
Droplet speed	~20 m/s	~10 m/s	
Time duration	~0.3-0.7 s		1 s
Droplet concentration	~10^4 droplets or more per sneeze	~10^2-10^3 or more per cough	12 μL/s
Droplet diameter	10-1,000 μm		10-160 μm

Table S2. Number of images and droplets analyzed for **Fig. 8** in the main text.

Sample	Number of images	Number of droplets
Control	13	5,167
Gauze	51	16,688
Lint-free wipe	58	4,524

Table S3 Concentrations of modifiers (acids and copper ions) detected in the 10-mL water reservoir (**Fig. S9**) after simulated inhalation tests in 99% RH through damp wipes.

Experimental condition	Concentration of modifiers in reservoir		"Inhalation" dosage of Cu (mass/volume of "inhaled" air) *
	pH	Cu	
Unmodified wipe, 6 m/s for 10 min	6.97	1.54 ppb	9.58×10^{-10} μg/cm^3
0.2 m/s for 1 h	5.62	2.52 ppb	7.87×10^{-9} μg/cm^3
1 m/s for 1 h	5.62	3.96 ppb	2.47×10^{-9} μg/cm^3
6 m/s for 10 min	5.06	53.23 ppb	3.32×10^{-8} μg/cm^3

* Inhalation dosage (μg/cm^3) was calculated by dividing the amount of detected copper ion (μg) by the product of airflow speed (m/s), duration of the flow (s) and the cross-sectional area of the gas tube (0.28 cm^2). In comparison, the mean copper concentration in natural water is around 60-150 ppb, and the upper limit of Cu level in drinkable water is 20 ppm.[4] Recommended dietary Cu allowance is around 500 μg.[5]

Table S4. Information of lint-free wipes and gauzes.

	Composition	Thickness (mm)	Packing density
Lint-free wipe	45% cellulose/ 55% polyester	0.29 ± 0.03	19%
Gauze	Polyester	0.36 ± 0.06	11%

Supplemental Experimental Procedures

Materials and parameters. Table S1 compares the parameters for coughing and sneezing with our experimental conditions. The airflow speed was measured by pointing a hot wire anemometer (Fishier Brand Traceable) next to the sprayer when it was not filled with any liquid. When filled with liquid, the flux of liquid ejection was measured by spraying the liquid to a container for 10 seconds and measuring the mass of the received liquid. As shown by the table, the experimental condition is comparable to that of coughing and sneezing.

To test if the substrate fabric is breathable enough, the pressure drop (pressure difference between the upstream and downstream) was measured at different airflow speeds. The fabrics to be measured were clamped between two chambers with a hot wire anemometer inserted in the downstream chamber to measure the airflow speeds. A manometer (Control Company #3461) was employed to obtain pressure difference between the upstream and downstream chambers. A lint-free wipe, a gauze, and a commercial mask (VWR maximum protection mask, VWR north America #414004-670) were tested. The result in **Fig. S1** indicates the lint-free wipe is as breathable as the commercial mask. The packing density of gauze is so low that no detectable pressure drop was obtained.

Fig. S2 demonstrates the optical microscopic images in transmission mode for fabrics used in this work. The fibers remained randomly distributed before and after coating with polyaniline. The gauze showed a lower fiber packing density compared to the lint-free wipe. The packing density of the two fabrics was measured as the ratio of fiber density to apparent density. Fiber density was obtained by immersing the fabric in water and weighing the water excluded with the density kit on a balance. Apparent density was got by measuring the mass of the fabric with known dimensions. The results were organized in **Table S4**.

Drying stain of droplets. The size of droplet was obtained by measuring the diameter of drying stain on the detector film, which is only reasonable when the drying stain has the similar size to the droplet itself, and when the contact angle is not too large or too small. In **Fig. S3a** and **S3d**, both unmodified and modified droplet have similar contact angles of around 60°. The images were obtained by pipetting a 10-μL model fluid droplet on the detector screen and taking photo with a smartphone (iphone 7 plus). For the image of modified droplet, the pH of the model fluid was adjusted to 1 with addition of phosphoric acid. The modified droplet looked green due to the reflection from the doped polyaniline. The microscopic top view of 2 μL of unmodified and modified droplet before and after drying are shown in **Fig. S3b** and **3c**, **3e** and **3f**, respectively. The drying stain had the same size as the droplet itself did in both situations. The drying stain looks a little bit different from those in **Fig. 5** because the droplet in **Fig. S3** (2 μL) is much larger than droplets from the sprayer.

Image processing. The processes of quantifying the contrast (*i.e.*, degree of modification) of each droplet with Matlab are illustrated in **Fig. 6** in the main text. Before executing the circle finding program, the original optical microscopy image in reflection mode was processed with a series of filters, in the order of grayscale, Gaussian blur, color inversion and binarization. In this process, grayscale reduced the dimension of images from 3 to 1, Gaussian blur worked as a noise reduction filter, color inversion satisfied the default setting of the algorithm, and binarization maximized the gradients of intensities of pixels at the edge of the droplets. After these pretreatments, the circle locating program based on Hough circle transform was executed which yielded the positions and sizes of the droplets. Hough circle transform[6] reduced unwanted features from the background such as the rolling marks in **Fig. S4a**. If the pre-processed image (**Fig. S4b**) is directly

overlapped on images of transmission, artifacts such as those from the rolling tracks of the plastic film will be counted as droplets (**Fig. S4c**). This will lead to a lot of close-to-zero values of the calculated degree of modification, which increases the level of noise in **Fig. 7** and **8**. With Hough circle transformation, droplets were approximated as circles and those high-aspect-ratio artifacts were removed, improving the overall accuracy of recognizing droplets. The droplet outlines were then overlapped on images of transmission to read the green channel intensity inside and outside droplets. For each droplet, the intensities values of pixels surrounding the circle were collected (the range is 5 pixels surrounding the outline of droplet) and the mode value was calculated to represent the brightness of the background. Next intensity values of pixels inside the droplet were collected and the average value of top 50% intensity values was calculated to represent the brightness of the droplet. The intensity values were averaged over the top 50% but not all intensity to avoid picking pixels outside the droplet as the droplet is not a perfect circle. Then degree of modification for this droplet was calculated according to **Eq. 1**. Matlab codes are available upon requests. The number of droplets and images analyzed are summarized in **Table S2**.

Eq. 1 is justified as follows. In the form of emeraldine, polyaniline exhibits green color upon being doped (emeraldine salt) and turns to blue in neutral to basic condition (emeraldine base). This color shift is due to the shift of absorption band. As a droplet lands on polyaniline, it dopes the polyaniline underneath. In transmission mode of optical microscope, the difference of absorbance of light gives the contrast of acidic droplet against the background, which is most obvious when the wavelength of light is in green range (500 to 600 nm) compared to blue and red range. The doped part of polyaniline was approximated as a cylinder with a cross section equaling to the droplet projection, and thickness of x, as illustrated in **Fig. S5**. The difference of light flux between the doped polyaniline and un-doped can be calculated according to Beer-lambert law:

$$\Phi_d^t = \Phi^i \exp(-\mu_{EB}(H - x) - \mu_{ES}x) \text{ (Eq. S1)}$$

$$\Phi_b^t = \Phi^i \exp(-\mu_{EB}H) \text{ (Eq. S2)}$$

$$\exp\big(x \cdot (\mu_{EB} - \mu_{ES})\big) = \frac{\phi_d^t}{\Phi_b^t} \text{ (Eq. S3)}$$

where Φ^t_d is the flux of transmitted light for a pixel inside a droplet, Φ^t_b is the flux of transmitted light for a pixel belonging to the background, Φ^i is the incoming light flux, H is the thickness of the film, x is the thickness of the green emeraldine salt region, and μ_{EB} and μ_{ES} are attenuation coefficients for emeraldine base and emeraldine salt, respectively. The left-hand side of **Eq. S3** is intrinsically determined by the pH of the droplet. The computer does not store the light intensity directly, instead, it is converted to pixel intensity according to:

$$I = C \times \Phi^t + C' \quad \text{(Eq. S4)}$$

Where I is the intensity for each pixel (ranging from 0-255), C is a constant determined by exposure time and gain, C' is determined by offset. By setting offset of the camera to zero, we have:

$$\frac{\phi_d^t}{\Phi_b^t} = 1 + \frac{I_d^P - I_b^P}{I_b^P} = 1 + Degree\ of\ modification \text{ (Eq. S5)}$$

Where I_d^P is the intensity of a pixel inside the droplet, I_b^P is the intensity of a pixel belong to the background. The physical meaning of degree of modification is related to the difference of light absorption band between acidic (under modified droplets) and neutral (background) area of polyaniline. Droplets are made of thousands of pixels, thus statistical values from those pixels were used to calculate degree of modification for one droplet. For pixels inside droplet, those having the top 50% highest intensities were collected and averaged, the value of which was used for I_d in **Eq. 1**. For pixels surrounding the droplets, the mode value was used for I_b.

Filtration efficiency and escaped droplets. Masks belong to the topic of gas phase filtration, where a model based on single fiber efficiency has been established to explain the mechanism of collection[7,8]. The overall efficiency of the filter, E, is related to the single fiber efficiency by

$$E = 1 - \exp\left(-4\varphi \frac{\alpha}{1-\alpha} \frac{z}{\pi d_f}\right) \text{ (Eq. S6)}$$

Where α is the packing density, z is the thickness of the filter, and d_f is the diameter of the fiber. φ is the single fiber collection efficiency of a fibrous media, defined as the ratio of flux of particles collected to the flux of particles approaching the fiber. It can be expressed as:

$$\varphi = \eta \cdot h \quad \textbf{(Eq. S7)}$$

Where η is the collision efficiency (note not to be mixed with modification efficiency defined in the main text) and h is the adhesion efficiency. η reflects how many of the incoming droplets collide with fibers and it is usually the dominant factor in determining the filtration rate of a filter. η can be evaluated from five mechanisms: interception, inertia impaction, diffusion, sedimentation, and electrostatic force. η is a function of droplet size. For droplets in micrometer scale, larger droplets can be better captured compared to smaller one due to more efficient interception and inertial impaction. For droplets colliding with fiber, they can either stay on the fiber or bounce off, which is represented by adhesion efficiency h. In generally, a higher speed and large particle size tend to decrease the adhesion efficiency[8,9], which is the reason why masks designed for breathing may be less efficient for coughing. With the addition of modulation layer, however, this problem can be largely mitigated as colliding droplets are modified upon contact with the fibers. Type (2) penetration (**Fig. 9**) corresponds to $\eta(1-h)$. Different from type 1, this part of penetration is expected to be modified droplets.

The model does not consider the interaction between fiber-fiber, particle-particle, and particle-fiber interactions. The collected aerosols can detach from the fibers due to those interaction, especially for liquid aerosols as they can slide, coalesce, and grow larger[9,10], which is defined as type (3). Type (3) cannot be easily expressed in the single fiber model as it is a result of interactions in a bulk material. Collected droplets can be observed either as large droplets or even a liquid film bridging neighboring fibers (**Fig. S6**). After spraying to the polyaniline coated gauze and wipe for 1 s, the two cases were observed under optical microscope immediately. For the gauze, individual coalesced droplet hung on a fiber with large contact angle. Captured droplets on the lint-free wipe, however, formed liquid pools covering fibers, which was a result of high capture rate and short distance between fibers. Regardless of how they are captured, they can be reemitted, either immediately or after incubation time, especially at high airflow speeds. In our experiment, the immediately released droplets were observed. In practice, reemission will be more obvious after the mask is used for a while, which is one of the reasons high-grade mask is not recommended for long time use. The chemical modulation layer can significantly reduce the risk caused by re-entrainment.

The quality factor is defined as[11]:

$$Q = -\ln(1-E)/\Delta P \quad \textbf{(Eq. S8)}$$

Where E is the total efficiency, and ΔP is the pressure drop. A high quality factor is important for respiratory filtration as attempts to increase the total efficiency must not sacrifice breathability. From the **Eq. S6**, we know that the total efficiency can be increased by increasing the packing density, thickness, and single fiber efficiency, or decreasing the diameter of fiber. However, increasing the packing density and thickness will inevitably increase the pressure drop and reduce the quality factor. In our work, none of the parameters were significantly changed before and after coating. However, instead of filtration rate, if we consider the total removal rate which includes both captured droplets and escaped but non-infectious droplets, then φ can be replaced with a higher value of φ'. This increase will be reflected in the increase of total removal efficiency. And one can have a higher removal rate and thus a higher quality factor without any increase in pressure drop. The modification efficiency we measured for gauze and lint-free wipe is the experimental result of $(E(\varphi')-E(\varphi))/(1-E(\varphi))$, which increases with increasing packing density and thickness. Although the gauze is slightly thicker, the packing density is much smaller than the lint-free wipe. This explains the higher modification efficiency for wipe compared to the gauze.

Detection of Cu in escaped droplets. Neocuproine (Nc) is usually used as a color indicator for the titration of Cu(I) ion[12,13]. We found that it is fluorescent, and its fluorescence can be quenched by Cu (II) ions both in the aqueous media (**Fig. S7**) and in a solid matrix. In **Fig. S7**, Nc was dissolved in ethanol at a concentration of 25 mg/mL. With an addition of a few mL of 0.1 M $CuSO_4$ solution, fluorescence quenching was readily observed. A UV lamp (c.a. 360 nm) was placed at the right side of the vial in **Fig. S7** as the source of excitation.

To prepare the fluorometric detector film, poly(methyl methacrylate) (PMMA, Mw ~350,000) was dissolved in anisole at a concentration of 10 mg/mL followed by dissolving Nc at a concentration of 25 mg/mL. The solution was spin-coated on a cover glass (2,000 rpm for 1 min). To calibrate the imaging contrast of droplet stains visualized under fluorescence quenching microscopy (FQM) with the concentration of copper ions, droplets with known concentrations of copper ions from 10^{-5} to 10^{-3} M were sprayed onto the film. It is found that droplets start to leave dark stains with obvious contrast when the Cu concentration is larger than 10^{-4} M (**Fig. S8**). Therefore, the droplets leaving those visual dark stains in **Fig. 10** should contain at least higher than 10^{-4} M of Cu^{2+}, which was found to be sufficient to deactivate influenza viruses.[14]

Control experiments simulating inhalation. The experimental setup to simulate inhalation is shown in **Fig. S9**. For "dry air" conditions, ambient air (23 °C, 40% RH) at an airflow speed of 0.2 m/s was pulled through an unused, $CuSO_4$-loaded gauze by a house vacuum. The downstream air was then guided into a tube containing 3 mL of deionized water. The same process was repeated on a pristine gauze. The concentrations of Cu from Cu-loaded gauze and pristine gauze in deionized water were analyzed to be 2.16 ppb and 1.73 ppb by inductively coupled plasma mass spectrometry (ICP-MS).

Additional experiments were carried out to detect any possible release of either copper ions or acids through damp masking layers by highly humid airflows. An ultrasonic humidifier was used to increase the humidity to 99% RH, as indicated by the humidity sensor placed in the upstream chamber. The humid air was drawn through the masking layer, passing through a downstream chamber before going through a 10 mL of deionized water reservoir in a tube. If any copper salts or acids were released to the downstream air, they should be dissolved in the water reservoir. $CuSO_4$- and H_3PO_4-loaded lint-free wipes were tested. They were first dampened with model respiratory fluid by 1 second of spraying. The airflow speeds were measured by a hot wire anemometer placed at the outlet of the downstream chamber without the fabrics. The reservoir in the gas wash tube was analyzed after passing humid air through for a predetermined duration. Cu ions and acids were detected by ICP-MS and a pH meter, respectively. The process was repeated on a pristine unmodified wipe at 6 m/s for 10 min as a control. The results were summarized in **Table S3**.

Color indication and rechargeability. After extensive spraying, the acid loaded on fabrics will be depleted. Depleted region has a darker color compared to acid rich area due to same principle of color change in the detector film. This can be used as an indicator of the level of acids remaining on the layer. Once depleted, acids can be reloaded onto the layer by immersing in acidic solution, which converts the color of the fabric layer back to green (**Fig. S10**). The gauze in the image was first sprayed continuously for 1 min, which depleted the loaded acids and darkened the color. It was then immersed in phosphoric acid solution (pH 1) again for re-doping. After 30 min, the re-doped gauze was rinsed in ethanol. After drying, the color was recovered back to green.

Supplemental References

1. Mittal, R., Ni, R., and Seo, J.-H. (2020). The flow physics of COVID-19. J Fluid Mech *894*, F2.
2. Han, Z.Y., Weng, W.G., and Huang, Q.Y. (2013). Characterizations of particle size distribution of the droplets exhaled by sneeze. J R Soc Interface *10*, 20130560.
3. Bourouiba, L., Dehandschoewercker, E., and Bush, J.W.M. (2014). Violent expiratory events: on coughing and sneezing. J Fluid Mech *745*, 537-563.
4. Gaetke, L.M., and Chow, C.K. (2003). Copper toxicity, oxidative stress, and antioxidant nutrients. Toxicology *189*, 147-163.
5. Fact Sheet for Health Professionals: Copper. https://ods.od.nih.gov/factsheets/Copper-HealthProfessional/ (September 30, 2020).
6. Kimme, C., Ballard, D., and Sklansky, J. (1975). Finding Circles by an Array of Accumulators. Commun ACM *18*, 120-122.
7. Thomas, D., Charvet, A., Bardin-Monnier, N., and Appert-Collin, J.-C. (2017). Aerosol filtration (ISTE Press - Elsevier).
8. Maus, R., and Umhauer, H. (1997). Single fibre collection and adhesion efficiency for biological particles. Part Part Syst Char *14*, 250-256.
9. Gac, J.M., and Gradon, L. (2012). Analytical investigation and numerical modeling of collisions between a droplet and a fiber. J Colloid Interface Sci *369*, 419-425.
10. Zhang, R.F., Liu, B.F., Yang, A.K., Zhu, Y.Y., Liu, C., Zhou, G.M., Sun, J., Hsu, P.C., Zhao, W.T., Lin, D.C.*, et al.* (2018). In Situ Investigation on the Nanoscale Capture and Evolution of Aerosols on Nanofibers. Nano Lett *18*, 1130-1138.
11. Liu, H., Cao, C.Y., Huang, J.Y., Chen, Z., Chen, G.Q., and Lai, Y.K. (2020). Progress on particulate matter filtration technology: basic concepts, advanced materials, and performances Nanoscale *12*, 437-453.
12. Apak, R., Guclu, K., Demirata, B., Ozyurek, M., Celik, S.E., Bektasoglu, B., Berker, K.I., and Ozyurt, D. (2007). Comparative evaluation of various total antioxidant capacity assays applied to phenolic compounds with the CUPRAC assay. Molecules *12*, 1496-1547.
13. Larsen, E.R. (1974). Spectrophotometric Determination of Copper in Fertilizer with Neocuproine. Anal Chem *46*, 1131-1132.
14. Horie, M., Ogawa, H., Yoshida, Y., Yamada, K., Hara, A., Ozawa, K., Matsuda, S., Mizota, C., Tani, M., Yamamoto, Y.*, et al.* (2008). Inactivation and morphological changes of avian influenza virus by copper ions. Archives of Virology *153*, 1467-1472.